Cell Reports
Medicine

Article

Overcoming multidrug resistance in gastrointestinal cancers with a CDH17-targeted ADC conjugated to a DNA topoisomerase inhibitor

Graphical abstract

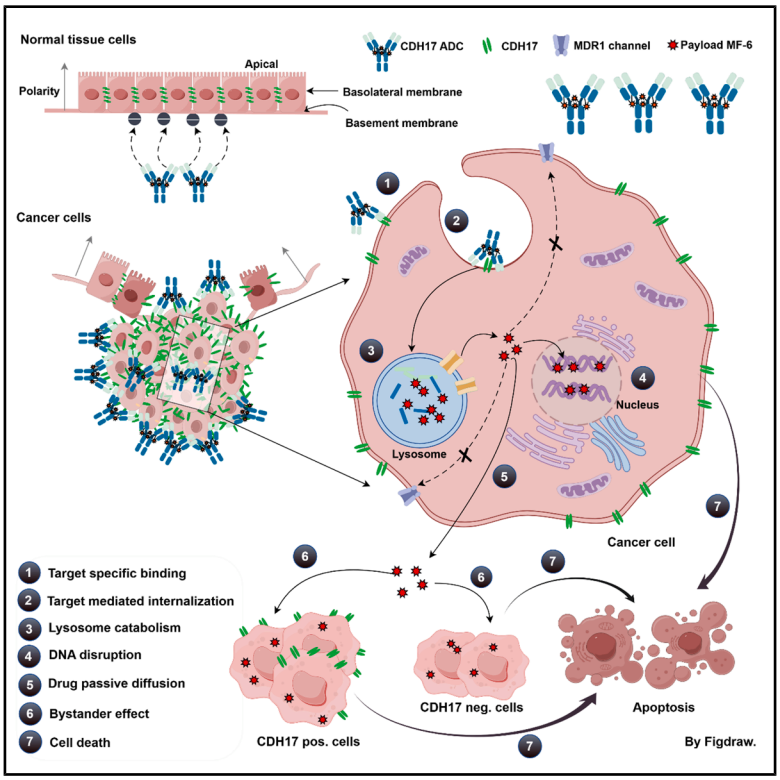

Highlights

- CDH17 emerges as a promising therapeutic target in GI cancers
- 7MW4911 is a CDH17-targeted ADC with a Top1 inhibitor MF-6
- 7MW4911 shows strong efficacy in GI cancer models, including MDR tumors
- 7MW4911 demonstrates a favorable safety profile in NHP toxicology studies

Authors

Rui Wang, Peng Fang, Xi Chen, ..., Datao Liu, Xiaoding Tan, Xun Gui

Correspondence

datao.liu@mabwell.com (D.L.), xiaoding.tan@mabwell.com (X.T.), xun.gui@mabwell.com (X.G.)

In brief

Wang et al. develop 7MW4911, a CDH17-targeted ADC carrying a Top1 inhibitor MF-6. 7MW4911 shows strong anti-tumor activity in diverse GI cancer models, including MDR tumors, and demonstrates a favorable safety profile in monkeys, supporting its potential for overcoming drug resistance and advancing to clinical development.

Wang et al., 2025, Cell Reports Medicine 6, 102213
July 15, 2025
https://doi.org/10.1016/j.xcrm.2025.102213

CellPress

Cell Reports Medicine

CellPress
OPEN ACCESS

Article

Overcoming multidrug resistance in gastrointestinal cancers with a CDH17-targeted ADC conjugated to a DNA topoisomerase inhibitor

Rui Wang,[1,5] Peng Fang,[1,5] Xi Chen,[1,2,5] Jiali Ji,[1] Dongan Yu,[1,3] Fei Mei,[1,3] Zhenzhen Wang,[1] Wei Zhou,[1] Wenjing Peng,[1] Rongjuan Wang,[1,4] Jian Wang,[1] Cuicui Guo,[1] Hai Wu,[1] Datao Liu,[1,2,*] Xiaoding Tan,[1,3,*] and Xun Gui[1,6,*]

[1]Mabwell (Shanghai) Bioscience Co., Ltd., Shanghai 201210, China
[2]National Engineering Laboratory for AIDS Vaccine, School of Life Sciences, Jilin University, Changchun 130012, China
[3]Jiangsu Mabwell Health Pharmaceutical R&D Co., Ltd., Taizhou 225300, China
[4]Beijing Kohnoor Science & Technology Co., Ltd., Beijing 102206, China
[5]These authors contributed equally
[6]Lead contact
*Correspondence: datao.liu@mabwell.com (D.L.), xiaoding.tan@mabwell.com (X.T.), xun.gui@mabwell.com (X.G.)
https://doi.org/10.1016/j.xcrm.2025.102213

SUMMARY

Cadherin 17 (CDH17) has emerged as a promising target for gastrointestinal (GI) cancers, which are often complicated by multidrug resistance (MDR) and recurrence. In this study, we developed 7MW4911, a CDH17-targeted antibody-drug conjugate (ADC) that incorporates a topoisomerase inhibitor MF-6 (Topi MF-6) payload linked via a cleavable linker, designed specifically to address MDR in GI cancers. 7MW4911 exhibited high specificity for CDH17-expressing cancer cells and potent cytotoxicity *in vitro*. In preclinical models, including patient-derived xenografts (PDXs) with distinct mutations, 7MW4911 achieved tumor growth inhibition ranging from 71% to 99%. Remarkably, 7MW4911 outperformed monomethyl auristatin E (MMAE)-based and Deruxtecan (DXd)-based ADCs in MDR models, highlighting its effectiveness against drug-resistant cancer phenotypes. Additionally, 7MW4911 showed favorable pharmacokinetics and a highest non-severely toxic dose (HNSTD) exceeding 20 mg/kg in cynomolgus monkeys, underscoring its promising safety profile. Together, these findings position 7MW4911 as a promising ADC candidate capable of enhancing therapeutic outcomes in GI cancers.

INTRODUCTION

Gastrointestinal (GI) cancers, including liver, gastric, pancreatic, neuroendocrine tumor (NET), and, the most prevalent, colorectal cancers, are among the leading causes of cancer-related mortality globally. According to the International Agency for Research on Cancer (IARC) GLOBOCAN statistics, these cancers account for approximately 24.6% of all cancer diagnoses and 34.2% of cancer deaths.[1] Globally, colorectal cancer (CRC) ranks third in overall cancer incidence and second in cancer-related mortality, while pancreatic cancer, though less common, had the highest mortality rate among all cancers in 2022. Despite this significant burden, effective screening strategies are limited primarily to colorectal, gastric, and esophageal cancers, resulting in many diagnoses at advanced stages where curative options are often unavailable. Additionally, nearly 50% of patients diagnosed at an early stage may experience disease recurrence, contributing to poor overall prognosis.[2,3] Although surgical interventions and postoperative chemoradiotherapy have reduced mortality rates, adverse reactions and drug resistance remain significant challenges. Immunotherapy has emerged as a promising treatment, but its effectiveness is currently restricted to a small subset of patients, highlighting the need for better predictive and prognostic biomarkers in GI cancers.[4]

Antibody-drug conjugates (ADCs) are advanced oncology therapies that combine monoclonal antibodies with cytotoxic drugs, targeting specific cancer cell antigens to selectively destroy malignant cells while sparing healthy tissues.[5–7] Since the approval of Mylotarg (gemtuzumab ozogamicin) for acute myeloid leukemia in 2000, 16 ADCs have been approved for various cancers, including T-DM1 (trastuzumab emtansine) and T-DXd (trastuzumab deruxtecan) for HER2-positive metastatic breast cancer.[8–11] Ongoing advancements in payloads, linkers, and coupling methods are improving the stability and efficacy of ADCs, enhancing their clinical applications and effectiveness in cancer treatment.[12–14] Among GI cancers, CRC is the most prevalent and has driven the development of multiple ADCs targeting diverse tumor-associated antigens and CRC phenotypes. Notable examples include the CEACAM5 ADC (M9140), B7-H3 ADC (HS-20093), and HER2 ADC (T-DXd). Among these, T-DXd has shown considerable promise. Recent results from the DESTINY-CRC02 study indicated an objective response rate of 37.8% in patients with HER2-positive, RAS wild-type, or mutant metastatic CRC (mCRC) who had

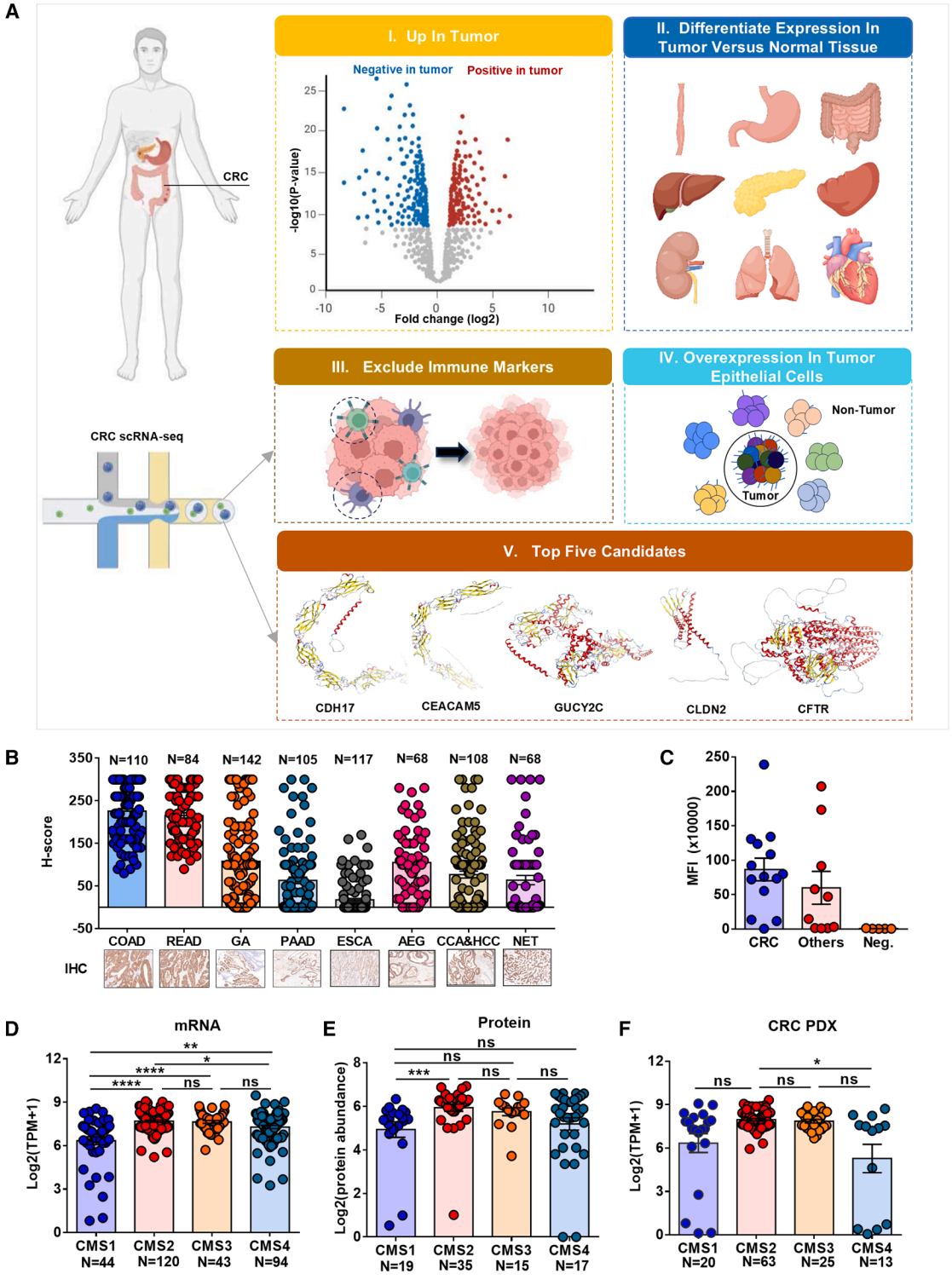

Figure 1. Identification of CDH17 as a potential therapeutic target for GI cancers

(A) Schematic overview of the multi-omics strategy for identifying gastrointestinal cancer markers. Key steps included (I) selection of genes upregulated in tumors vs. normal tissues, (II) exclusion of genes highly expressed in normal organs (organ images from Figdraw), (III) removal of markers expressed on immune cells, and (IV) identification of tumor epithelium-specific genes. The top five colorectal cancer candidates and a representative simulated protein structure are shown (V). Statistical analyses were performed in R 4.2.2.

(legend continued on next page)

previously received standard chemotherapy, highlighting its strong anti-tumor activity and favorable safety profile.[15] However, HER2 mutations account for only 3%–5% of CRC, and HER2-directed therapy is only indicated for patients with HER2-amplified tumors with wild-type RAS/RAF.[16] Other therapeutic targets also face challenges, including potential toxicity to normal tissues. Therefore, there is an urgent need to identify clinically actionable targets and develop innovative strategies to address unmet clinical needs and improve the quality of life for individuals with CRC.

Cadherin 17 (CDH17), or liver-intestine cadherin (LI cadherin), is a member of the 7D-cadherin superfamily, distinguished by seven cadherin-type repeats and a short 20-amino-acid cytoplasmic domain.[17] During embryogenesis, CDH17 is expressed in the fetal liver and GI tract, with physiological expression primarily in small intestine and colon epithelial cells. Functionally, it plays a vital role in intercellular adhesion, tissue integrity, intestinal peptide transport, and calcium-dependent water absorption.[18,19]

Aberrant expression of CDH17 is closely associated with the development, progression, and metastasis of various GI cancers.[20–22] CDH17 promotes tumorigenicity by regulating the Wnt/β-catenin and mitogen-activated protein kinase (MAPK) signaling pathways, driving cell proliferation, survival, and migration.[23,24] It also interacts with integrin signaling to enhance cell adhesion and motility, contributing to tumor progression, particularly in CRC.[25] Studies have shown that CDH17 is highly expressed in metastatic tumors, and blocking CDH17 can significantly reduce lung metastasis in hepatocellular carcinoma and gastric carcinoma.[26–28] Additionally, CDH17 may be targeted in cancer therapy based on specific biomarkers in tumor tissue or serum.[29] Transcriptomic and proteomic analyses underscore its potential as a leading therapeutic target in CRC, correlating its expression with tumorigenicity and immune response.[30] Several CDH17-targeted antibody-based therapies are currently in early development stages for treating GI cancers. These include bispecific antibodies such as BI905711 (Boehringer Ingelheim) and ARB202 (Arbele), along with CDH17-based CAR therapies like CHM 2101 (Chimeric Therapeutics).[31,32] Additionally, several companies are exploring the potential of developing ADCs targeting CDH17 for the treatment of GI cancers, particularly CRC, which are prone to developing drug resistance following treatment. Although CDH17-based therapeutics are currently in the early stages of clinical trials or development, it remains unclear whether CDH17 is an optimal target, especially as an ADC target. Furthermore, the development of anti-CDH17 ADCs must address the challenge of multidrug resistance (MDR) in GI cancers to improve clinical outcomes for patients.

In this study, we demonstrate that CDH17 is highly expressed across GI cancers, with nearly 100% expression observed in clinical samples from CRCs and 23%–88% expression in other GI cancers. This substantial expression underscores the therapeutic potential of targeting CDH17. We have developed an anti-CDH17 ADC, designated 7MW4911, that incorporates our proprietary topoisomerase inhibitor MF-6 (Topi MF-6) payload designed to target MDR in GI cancers. Utilizing a site-specific conjugation strategy with IDconnect technology, 7MW4911 achieves a homogeneous drug-to-antibody ratio (DAR) of 4 products, enhancing its therapeutic efficacy. Preclinical evaluations of 7MW4911 reveal potent tumoricidal activity and significant inhibition of tumor growth in various cell line-derived xenograft (CDX) and patient-derived xenograft (PDX) models of GI cancers. Favorable pharmacokinetics (PK) and safety profiles were observed in non-human primate (NHP) studies. The ongoing evaluation of 7MW4911 will provide vital insights into its efficacy and safety, potentially paving the way for its clinical application in the management of GI cancers.

RESULTS

CDH17 as a prominent therapeutic target for GI cancers

A multi-omics approach was employed to identify potential ADC targets for GI cancers, with a focus on CRC. By integrating transcriptomics and proteomics data, we characterized gene and protein expression patterns across GI tumors and associated tissues, enabling the identification of clinically relevant targets. The application of these methodologies to GI cancers, including CRC, consistently identified *CDH17* as the lead candidate. Here, we delineate the key steps in the identification of CRC therapeutic targets. Initially, we performed differential gene expression analysis using The Cancer Genome Atlas (TCGA) datasets, identifying genes significantly upregulated in tumor tissues (Figure 1AI). Candidate selection was then refined by prioritizing cell surface proteins and cross-referencing their expression profiles with normal tissue datasets from the Genotype-Tissue Expression (GTEx) project and the Human Protein Atlas (HPA). This approach enabled the exclusion of genes with high expression in 33 normal tissues, ensuring tumor selectivity (Figure 1AII). Single-cell RNA sequencing (scRNA-seq) validation confirmed the predominant expression of the remaining candidates in malignant cells. This rigorous selection process yielded five potential CRC biomarkers: *CDH17*, *CEACAM5*, *GUCY2C*, *CLDN2*, and *CFTR*. *CDH17* emerged as the most promising candidate due to its tumor-specific expression profile and minimal on-target expression (Figures 1AIII–1AV and S1A–S1D). Further pan-cancer analysis using TCGA and GTEx datasets validated

(B) CDH17 expression analysis in gastrointestinal cancer tissue microarrays. H-scores and sample numbers are detailed in Table S1. Representative IHC images show variable staining intensities. Data are represented as mean ± SEM.

(C) CDH17 surface expression in gastrointestinal cancer cell lines, as assessed by flow cytometry. Negative controls included primary endothelial cells and non-cancerous cell lines. Data are represented as mean ± SEM.

(D and E) CDH17 mRNA (D) and protein (E) expression levels across CRC CMS1–4 subtypes using TCGA and clinical sample data, respectively. Data are presented as mean ± SEM.

(F) Summary of CDH17 expression in CRC PDX models by molecular subtype. Data are represented as mean ± SEM.

Statistical significance was determined by Kruskal-Wallis test in (D)–(F). $^{*}p < 0.05$, $^{**}p < 0.01$, $^{***}p < 0.001$, and $^{****}p < 0.0001$. See also Figures S1 and S2 and Table S1.

CDH17's specificity for GI malignancies, particularly CRC, supporting its therapeutic potential (Figure S1E).

To further characterize the protein expression profile of CDH17 in GI cancers, we conducted immunohistochemistry (IHC) analysis on tissue microarrays from various GI malignancies. Our results demonstrated that CDH17 was highly expressed across GI malignancies, particularly in colon cancer (colon adenocarcinoma [COAD]) and rectal adenocarcinoma (READ), where all tested samples exhibited 100% positivity, with H-scores ranging from 50 to 300 (Figure 1B). Positive CDH17 expression (H-score > 15) was also observed in gastric adenocarcinoma (GA) (77%), pancreatic adenocarcinoma (PAAD) (55%), esophageal carcinoma (ESCA) (23%), adenocarcinoma of the esophagogastric junction (AEG) (88%), cholangiocarcinoma and hepatocellular carcinoma (CCA and HCC) (59%), and NETs (44%) (Figure 1B; Table S1). In contrast, CDH17 expression in normal tissues was minimal, with notable staining primarily observed in the epithelial cells of the small intestine, colon, and appendix (Figure S2A). To assess the potential for on-target, off-tumor toxicities, we further examined CDH17 expression in normal intestinal tissues using tumor tissue microarrays, revealing a significant difference between malignant and normal intestinal tissues (Figure S2B). Although derived from non-matched tumor-normal samples, these data provide a representative comparison across tissue types. Publicly available data from the GEPIA database further validated the differential expression of CDH17 between cancerous and normal tissues (Figure S2C). Notably, a previous study has shown that CDH17 is predominantly localized to the basolateral membrane of GI epithelial cells.[32] This restricted distribution minimizes ADC accessibility in normal tissues, thereby reducing the risk of on-target, off-tumor toxicities and suggesting CDH17 as a viable therapeutic target for ADC-based cancer treatment. Flow cytometry analysis further confirmed high and specific CDH17 expression in GI cancer cell lines, including those derived from COAD, GA, PAAD, and HCC (Figure 1C). Collectively, these findings establish CDH17 as a promising therapeutic target in GI cancers, particularly CRC, due to its tumor-specific expression, minimal presence in normal tissues, and reduced potential for on-target, off-tumor toxicities. These characteristics support the development of CDH17-targeted ADC therapies for GI malignancies.

Ongoing research seeks to identify biologically distinct subtypes of CRC to improve prognostic accuracy and guide the development of targeted therapies. The Colorectal Cancer Subtyping Consortium (CRCSC) has classified CRC into four consensus molecular subtypes (CMSs) based on transcriptomic analysis: CMS1 (immune activated), CMS2 (canonical, characterized by Wnt/Myc pathway activation), CMS3 (metabolic, with KRAS mutations), and CMS4 (mesenchymal, associated with transforming growth factor beta [TGF-β] pathway activation). Each subtype presents distinct biological features that are critical for optimizing treatment strategies.[33] To explore the role of CDH17 in CRC, we analyzed its expression across these subtypes, hypothesizing that CMS2 would exhibit the highest expression due to its involvement in the Wnt/β-catenin signaling pathway. Our results revealed that CMS2 displayed the highest CDH17 protein expression, significantly higher than CMS1, while CMS3 showed comparable RNA expression levels. No significant difference in protein expression was observed between CMS2, CMS3, and CMS4 (Figures 1D and 1E). In addition, CDH17 expression in PDX models was higher in CMS2 compared to CMS4, with no significant difference between CMS2, CMS1, and CMS3 (Figure 1F). These findings confirm that CDH17 expression is most prominent in the CMS2 subtype, with consistent patterns observed across various data models.

These results underscore the therapeutic potential of targeting CDH17, particularly in CMS2 and CMS3 subtypes, and highlight the importance of selecting appropriate models for drug efficacy evaluation. Further investigations are needed to facilitate comprehensive comparisons across all CRC subtypes and inform the design of clinical trials targeting CDH17 in CRC.

Innovative development of the CDH17-targeted ADC 7MW4911

To develop a CDH17-targeted ADC, a panel of anti-CDH17 antibodies was generated, as outlined in the screening flowchart (Figure S3A). The lead antibody, the murine version of Mab0727, which binds to the EC1-2 domain of CDH17, demonstrated specific binding to tumor cells, high internalization efficacy, and a robust cytotoxic profile across various CRC cell lines in *in vitro* assays (Figure S3B). This antibody was subsequently humanized for further studies. Subsequent assays confirmed that Mab0727 displayed strong cross-reactivity with rhesus and cynomolgus monkey CDH17 but did not bind to CDH17 from other species, including mouse, rat, or canine (Figures S3C–S3E). The antibody demonstrated a moderate binding affinity for CDH17, as evidenced by bio-layer interferometry assay, and exhibited a high degree of specificity, showing no cross-reactivity with other members of the cadherin family (Figures S3F, S3G, S4A, and S4B).

The stability and PK profiles of Mab0727 were also evaluated. *In vitro*, Mab0727 exhibited good stability in cynomolgus monkey plasma, and *in vivo*, it displayed a favorable PK profile in BALB/c mice, with an estimated half-life ($t_1/_2$) of approximately 144 h (Figures S4C–S4F). Given its importance in ADC development, the hydrophobicity and thermal stability of Mab0727 were further assessed. The results indicated excellent hydrophilicity, as determined by hydrophobic interaction chromatography (HIC)-high-performance liquid chromatography (HPLC), and robust thermal stability across a range of pH conditions (Table S2). Collectively, Mab0727 is a highly specific anti-CDH17 antibody with favorable binding affinity to both human and NHP CDH17, as well as excellent biophysical stability, positioning it as an ideal candidate for ADC development.

The anti-CDH17 ADC 7MW4911 was developed by conjugating Mab0727 to the topoisomerase I inhibitor MF-6 using IDconnect technology, along with a protease-cleavable linker incorporating both the IDconnect structure and a Val-Ala dipeptide (Figure 2A). The IDconnect technology employs a substituted maleimide scaffold featuring 4-mercapto-benzoyl-morpholine as the leaving group at the 3 and 4 positions. This approach enables site-specific conjugation to Mab0727 by cross-linking the reduced cysteine residues in the Fab and hinge regions of the antibody.

CellPress
OPEN ACCESS

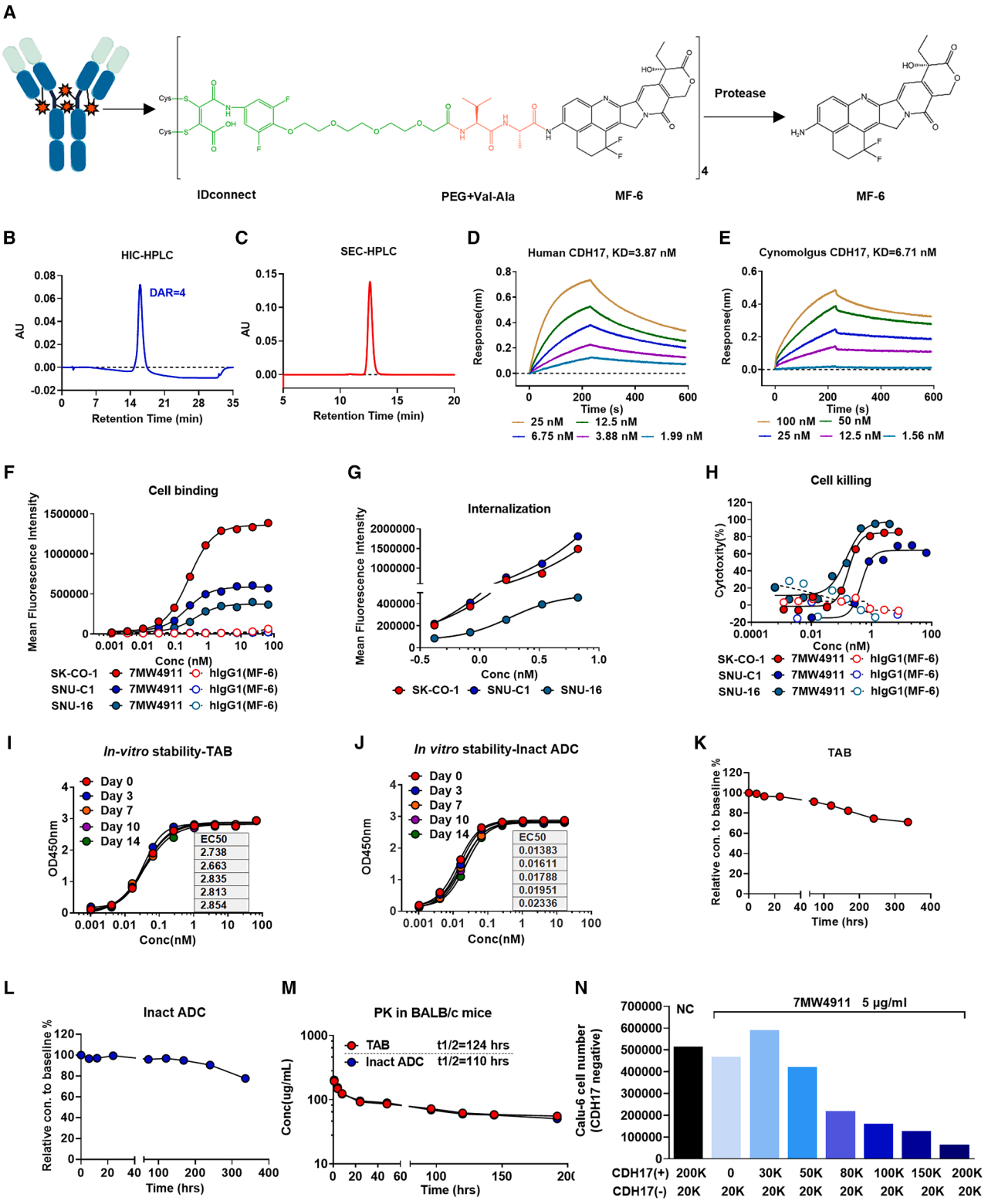

Figure 2. Generation and characterization of anti-CDH17 ADC 7MW4911

(A) Structure of 7MW4911: the ADC consists of the MF-6 payload conjugated to Mab0727 via a linker system composed of IDconnect and PEG-VA, enabling efficient payload release.

(B and C) Physicochemical properties of 7MW4911 were measured by HIC-HPLC (B) and SEC-HPLC (C).

(legend continued on next page)

Physicochemical profiling and comprehensive *in vitro* and *in vivo* functional characterization of 7MW4911

7MW4911 was site-specifically conjugated using IDconnect technology via inter-chain disulfide bonds, resulting in nearly 100% homogeneous DAR 4 products, as confirmed by HIC-HPLC and size-exclusion chromatography (SEC)-HPLC analysis (Figures 2B and 2C). The binding affinity of 7MW4911 for both human and cynomolgus CDH17 was comparable to that of its parental antibody, Mab0727 (Figures 2D, 2E, S3F, and S3G). Further evaluation of the hydrophobic properties and thermal stability of 7MW4911 revealed excellent hydrophilicity, as assessed by HIC-HPLC, and robust thermal stability across various pH conditions, matching that of Mab0727 (Table S2). These findings affirm the high quality and therapeutic potential of 7MW4911 for clinical applications.

The binding affinity, internalization capacity, and cytotoxic potency of 7MW4911 were evaluated in cell lines with varying levels of CDH17 expression. As expected, 7MW4911 exhibited specific binding to tumor cells, including colorectal and gastric cancer cell lines, and demonstrated efficient internalization (Figures 2F and 2G). Cytotoxicity assays confirmed that 7MW4911 effectively induced cell death in CDH17-positive cells compared to the control ADC, hIgG1(MF-6) (Figure 2H). Monomethyl auristatin E (MMAE), a widely used cytotoxic payload in ADC development, exerts its anti-tumor activity by disrupting microtubule polymerization, thereby promoting targeted cancer cell death. To assess the association between CDH17 expression levels and *in vitro* cytotoxic response, we employed an MMAE-conjugated form of Mab0727 as a reference comparator (Figures S5A–S5C). The CDH17-dependent nature of the cytotoxic effect was further validated since Mab0727(MMAE) demonstrated a positive correlation between cell-killing potency and the CDH17 copy number (Figures S5D and S5E). MMAE was selected based on its documented application in CDH17-targeted ADCs, as reported in patent WO2023107558A1. This comparison aimed to determine whether 7MW4911 conjugated with MF-6, a DNA topoisomerase I inhibitor, could deliver superior anti-tumor efficacy, particularly in CRC models exhibiting limited responsiveness to MMAE in subsequent *in vivo* studies.

The stability and PK profiles of 7MW4911 were comprehensively evaluated. *In vitro* binding assays demonstrated consistent OD_{450} readings and comparable EC_{50} values across samples incubated with cynomolgus monkey plasma for various time points (Figures 2I and 2J). Both total antibody (TAB) and intact ADC detection revealed that after 240 h of incubation with cynomolgus monkey plasma, 90% of the intact ADC remained intact, indicating the significant stability of 7MW4911 (Figures 2K and 2L). In BALB/c mice, 7MW4911 exhibited a favorable PK profile, with a $t_1/_2$ of approximately 110–124 h across two different measurement methods (Figure 2M).

To further validate the therapeutic potential of the 7MW4911 ADC, biodistribution studies were performed in the CRC LS513 CDX model to assess its tumor accumulation relative to other organs. Quantification of both TAB and intact ADC revealed preferential localization in tumor tissue over the heart, liver, lung, spleen, kidney, etc. (Figures S6A–S6D). Notably, intratumoral drug concentrations remained elevated for up to 240 h post-dosing, underscoring the sustained tumor-targeting capability of 7MW4911 and its potential for improved therapeutic efficacy.

Additionally, the bystander effect of 7MW4911 was assessed *in vitro*. As shown in Figure 2N, 7MW4911 exhibited potent cytotoxicity in the CDH17-negative cell line, suggesting that MF-6 effectively diffuses across cell membranes from CDH17-positive cells into the surrounding tumor microenvironment. These findings indicate a strong bystander effect of 7MW4911, which may enhance its therapeutic efficacy in heterogeneous tumor settings.

In summary, 7MW4911 demonstrated high-affinity target binding, efficient intracellular trafficking, and potent cytotoxic activity against tumor cells. Coupled with its favorable pharmacokinetic properties, metabolic stability, selective tumor accumulation, and a robust bystander effect, these findings collectively support 7MW4911 as a promising candidate for further clinical development in GI cancer therapy.

Exceptional anti-tumor efficacy of 7MW4911 in CRC CDX and PDX models

The *in vivo* anti-tumor efficacy of 7MW4911 was evaluated across multiple CRC xenograft models, with the dosing regimens outlined in Figure 3A. 7MW4911 demonstrated potent anti-tumor efficacy, achieving tumor growth inhibition (TGI) rates ranging from 29% to 97% across CRC CDX models with varying levels of CDH17 expression (Figure 3B; Table S3). The anti-tumor effect of 7MW4911 was positively correlated with CDH17 expression levels, and dose-dependent tumor inhibition was observed. The efficacy of 7MW4911 was highlighted in four out of nine CRC CDX models, showcasing its potential as a targeted therapy for CDH17-expressing tumors. In CDX models with high CDH17 expression, including SNU-C1 (H-score: 200) and LS513 (H-score: 240), 7MW4911 exhibited potent anti-tumor effects. In the SNU-C1 model, TGI rates of 79%, 91%, and 91% were observed at doses of 2.5, 5, and 10 mg/kg, respectively (Figure 3C), with tumor weight measurements aligning with

(D and E) Binding affinities of 7MW4911 to human (D) and cynomolgus monkey (E) CDH17 were measured by Octet RED96 system.
(F) Binding of 7MW4911 to CDH17-expressing cell lines (SK-CO-1, SNU-C1, SNU-16) was assessed by flow cytometry.
(G) CDH17-mediated internalization of 7MW4911 was evaluated in CDH17-positive cell lines.
(H) Cytotoxicity of 7MW4911 was measured in cell lines with varying CDH17 expression using CellTiter-Glo assays.
(I–L) Stability of 7MW4911 in cynomolgus monkey plasma. Binding activity (I and J) and concentrations (K and L) of total antibody (TAB) and intact ADC were evaluated over time, as described in the STAR Methods. Data in (K) and (L) are normalized to baseline values.
(M) Pharmacokinetics of 7MW4911 in BALB/c mice following a single intravenous dose on day 0. Serum levels of TAB and intact ADC were quantified over time. Data are represented as mean ± SEM (n = 4).
(N) Bystander killing effect of 7MW4911 evaluated using a co-culture model.
See also Figures S3–S6 and Table S2.

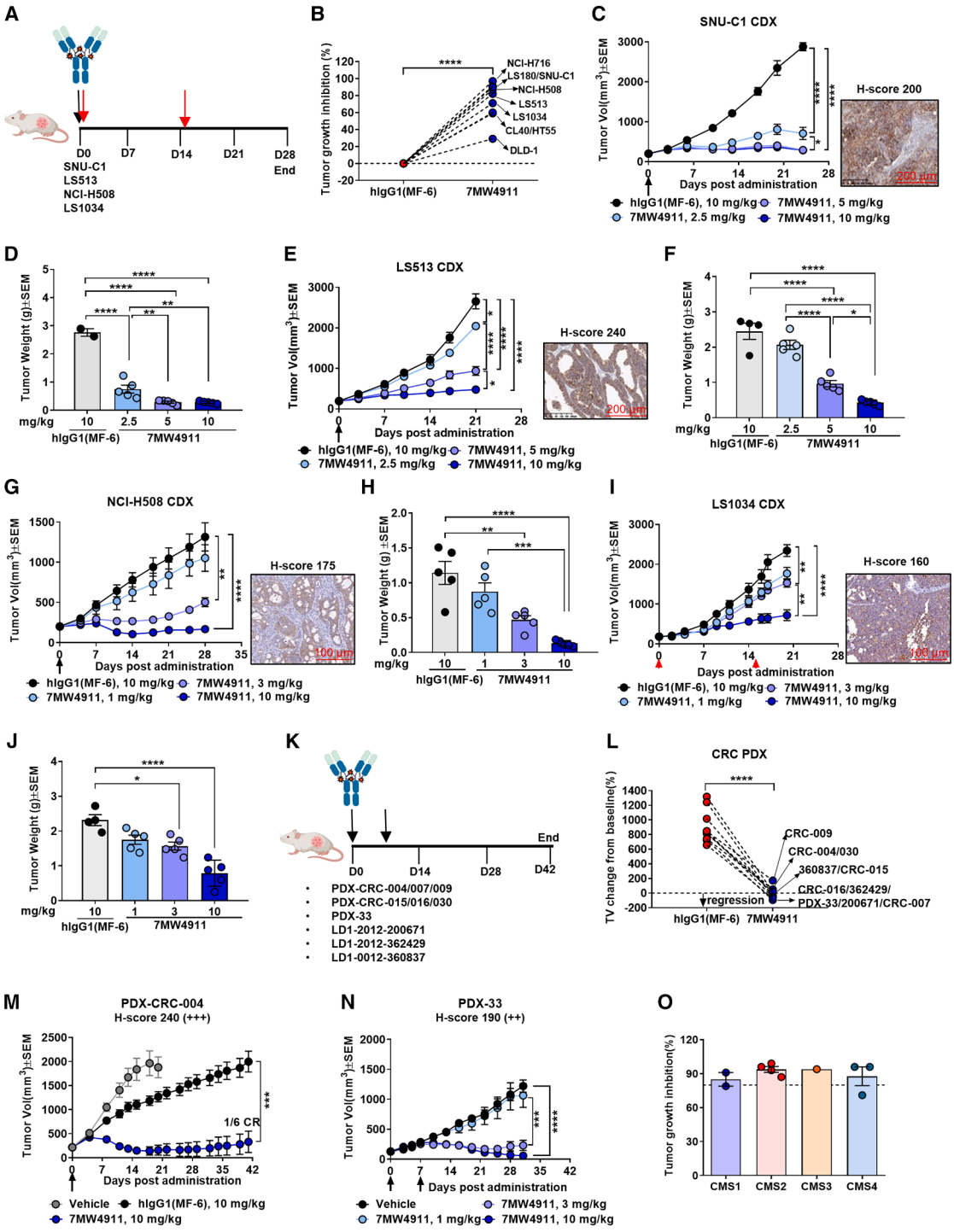

Figure 3. Potent anti-tumor activity of 7MW4911 in multiple CRC CDX and PDX models

(A) Schematic of the CRC CDX treatment regimen. Tumor-bearing mice received intravenous 7MW4911 or control ADC on day 0 (black or red arrows).

(B) TGI in CRC CDX models following 10 mg/kg 7MW4911 treatment.

(C–J) *In vivo* anti-tumor efficacy of 7MW4911 was evaluated in various CRC CDX models following the treatment regimen. *In vivo* anti-tumor efficacy of 7MW4911 in various CRC CDX models. Tumor volume and weight were measured in SNU-C1 (C and D; $n = 2–5$), LS513 (E and F; $n = 4–5$), NCI-H508 (G and H; $n = 5$), and LS1034 (I and J; $n = 4–5$). Data are represented as mean ± SEM. Mice were euthanized early if tumors exceeded 3,000 mm^3 (3 in SNU-C1 and 1 each in LS513 and LS1034).

(legend continued on next page)

tumor volume reductions (Figure 3D). Similarly, in the LS513 model, TGI rates of 23%, 65%, and 82% were observed in a dose-dependent manner (Figures 3E and 3F).

In moderate CDH17 expression models, including NCI-H508 (H-score: 175) and LS1034 (H-score: 160), 7MW4911 also demonstrated dose-dependent anti-tumor activity. In the NCI-H508 model, doses exceeding 1 mg/kg were effective, with TGI rates of 62% and 87% at 3 and 10 mg/kg, respectively (Figure 3G) and tumor weight measurements corroborating tumor volume reductions (Figure 3H). Similarly, in LS1034, TGI rates of 29%, 39%, and 71% were observed at 1, 3, and 10 mg/kg, respectively (Figures 3I and 3J). *Ex vivo* fluorescence-activated cell sorting (FACS) binding analysis of tumor cells recovered from these CDX models confirmed that 7MW4911 effectively bound to CDH17-expressing tumor cells, with binding potency correlating with tumor inhibition activity (Figures S7A–S7D). Although off-tumor, target-based toxicity could not be evaluated in rodent models due to the species-specific binding properties of the ADC, treatment with 7MW4911 did not result in significant body weight changes (Figures S7E–S7H), suggesting a favorable safety profile.

To evaluate the clinical potential of 7MW4911, its therapeutic efficacy was assessed in CRC PDX models. Mice were treated with either 7MW4911 or a control ADC, hIgG1(MF-6), as outlined in Figure 3K. Notably, 7MW4911 demonstrated robust anti-tumor activity across all tested models, exhibiting significant tumor inhibition regardless of CDH17 expression levels or underlying tumor genetic mutations (Figure 3L; Table S4). This efficacy was further supported by tumor growth curves and tumor weight measurements (Figures S8A–S8T). To illustrate its therapeutic potential, two representative CRC PDX models were highlighted. In the PDX-CRC-004 model (H-score: 240), 7MW4911 induced substantial tumor shrinkage, achieving a TGI of 93% by day 20 compared to the vehicle group with 84% by day 41 relative to the control ADC group (Figure 3M). Notably, one mouse exhibited complete tumor regression, with supporting data presented in Figures S8A and S8K. Similarly, in the PDX-33 model (H-score: 190), 7MW4911 demonstrated dose-dependent efficacy, with TGI rates of 82% and 96% at 3 and 10 mg/kg, respectively (Figure 3N, S8B, and S8L).

Further analysis evaluated the therapeutic efficacy of 7MW4911 across CMS1–4 of CRC within the PDX models. Preliminary results demonstrated that 7MW4911 exhibited anti-tumor activity across all CMS subtypes, irrespective of the subtype-specific CDH17 expression patterns (Figure 3O). Nonetheless, validation in larger cohorts is required to confirm these observations.

In conclusion, these findings highlight the robust and broad anti-tumor efficacy of 7MW4911 across diverse CRC models, including those with varying CDH17 expression levels, molecular subtypes, and genetic profiles. The demonstrated dose-dependent activity and efficacy across multiple models position 7MW4911 as a promising candidate for further clinical development in the treatment of CRC.

Promising *in vivo* potency of 7MW4911 in gastric and pancreatic cancers

In addition to CRC, CDH17 is highly expressed in a significant proportion of patients with gastric and pancreatic cancer, with average H-scores of 108 and 63, respectively (Figure 1B). To investigate the therapeutic potential of 7MW4911 in these malignancies, three gastric and one pancreatic CDX model was utilized (Figure 4A). In gastric cancer models, 7MW4911 exhibited robust anti-tumor activity, achieving TGI rates of 56%, 57%, and 95%, respectively (Figure 4B). Data from two models are highlighted here. In the SNU-16 model (H-score: 150), five out of six mice (5/6) achieved complete tumor regression, while the remaining mouse displayed substantial tumor shrinkage following a single 10 mg/kg dose of 7MW4911 (Figures 4C and 4D). Similarly, in the 23132/87 model (H-score: 135), 7MW4911 demonstrated significant efficacy with a TGI of 57% (Figures 4E and 4F). These results underscore the potential of 7MW4911 as a promising therapeutic candidate for gastric cancer.

To further evaluate the anti-tumor efficacy of 7MW4911 in gastric cancer, three PDX models were employed. In the LD1-2017-361697 model, a single 10 mg/kg injection of 7MW4911 achieved complete tumor regression in all three mice by day 32 (Figure 4G). In the other two models, 7MW4911 also exhibited substantial anti-tumor activity, achieving TGI rates of 69% and 91%, respectively (Figures 4H and 4I). Tumor weights measured at the study endpoint further supported these findings (Figure 4J). Collectively, these results highlight the potent therapeutic potential of 7MW4911 in clinically relevant gastric cancer models. Nonetheless, further evaluation across a broader spectrum of models is necessary to fully establish its clinical applicability.

For pancreatic cancer, the anti-tumor efficacy of 7MW4911 was also demonstrated. In the AsPC-1 CDX model, two doses of 3 mg/kg 7MW4911 resulted in an 81% TGI (Figures 4K and 4L), underscoring its effectiveness against pancreatic malignancies.

Taken together, these findings position 7MW4911 as a compelling therapeutic candidate for advanced GI cancers. With broad-spectrum efficacy, including complete tumor regression in the SNU-16 gastric cancer model and a gastric cancer PDX model, alongside significant tumor inhibition across additional gastric and pancreatic models, 7MW4911 demonstrates transformative potential. The precise tumor cell targeting demonstrated by 7MW4911 further bolsters its therapeutic promise, paving the way for its clinical development to address critical unmet needs in GI oncology.

(K) Schematic of the CRC PDX treatment regimen. Mice received intravenous administration of 7MW4911 or control ADC on day 0.
(L) Summary of tumor volume changes from baseline in CRC PDX models.
(M and N) Tumor volume changes in PDX-CRC-004 (n = 6) and PDX-33-F4-1 (n = 6–8). Data are represented as mean ± SEM.
(O) Efficacy summary of 7MW4911 across CMS1–4 subtypes in PDX models. CR, complete regression.
Statistical significance was determined using one-way ANOVA for all models except (B) and (L), which were analyzed using paired t tests. *$p < 0.05$, **$p < 0.01$, ***$p < 0.001$, and ****$p < 0.0001$. See also Figures S7 and S8 and Tables S3 and S4.

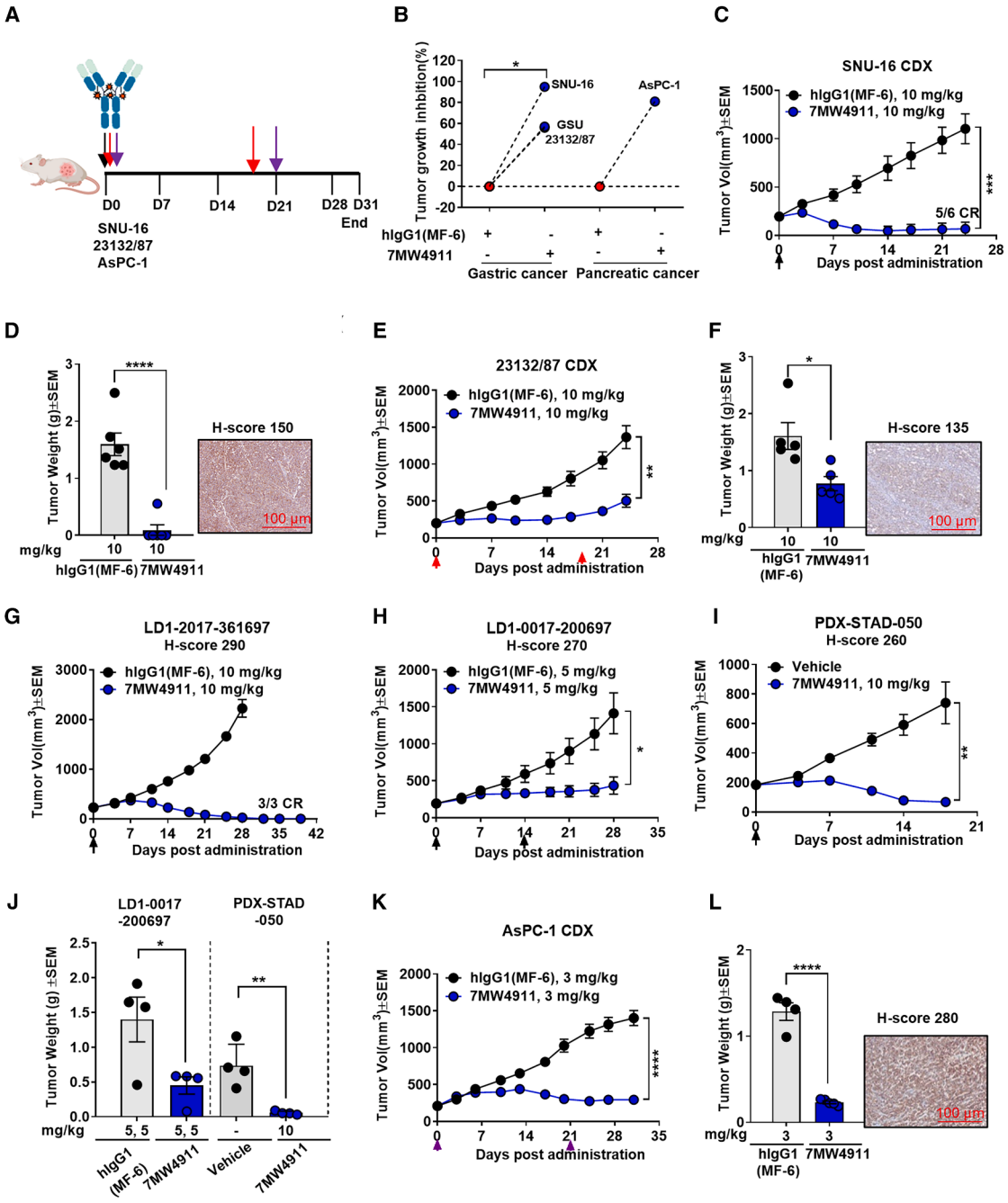

Figure 4. Impressive anti-tumor activity of 7MW4911 in gastric and pancreatic cancer models

(A) Schematic of treatment regimens in gastric and pancreatic cancer CDX models. Mice received 7MW4911 or control ADC on day 0 (black, red, or purple arrows).

(B) Summary of TGI following 10 mg/kg 7MW4911 in gastric cancer CDX models and 3 mg/kg in the pancreatic cancer CDX model.

(C–F) *In vivo* efficacy in gastric cancer CDX models: tumor volume and weight in SNU-16 (C and D; $n = 6$) and tumor volume and weight in 23132/87 (E and F; $n = 5$). Data are represented as mean ± SEM ($n = 6$).

(G–J) Tumor volume changes and tumor weights in three gastric cancer PDX models. One mouse in each group of the PDX-STAD-050 model died on day 18, probably due to tumor-related factors. Data are represented as mean ± SEM ($n = 3$–5). STAD, stomach adenocarcinoma.

(K and L) Efficacy in the AsPC-1 pancreatic cancer CDX model: tumor volume ($n = 5$) and weight ($n = 4$). Data are represented as mean ± SEM.

Statistical analysis was performed using unpaired two-tailed t tests except for (B), which was analyzed using paired t tests. CR, complete regression. *$p < 0.05$, **$p < 0.01$, ***$p < 0.001$, and ****$p < 0.0001$. See also Table S3.

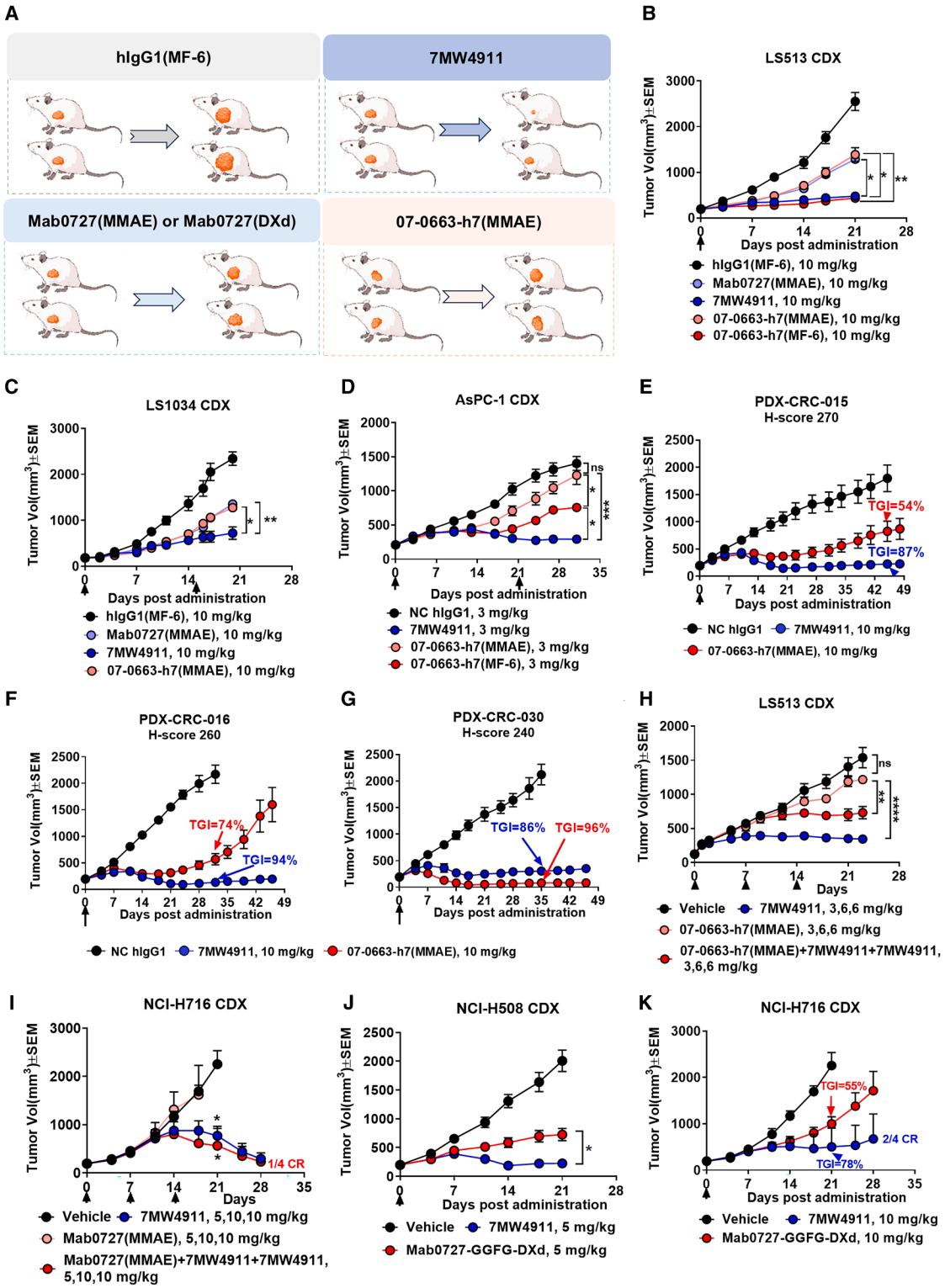

Figure 5. Strong anti-tumor efficacy of 7MW4911 in MDR models

(A) Schematic of MMAE-resistant models (created with Figdraw).

(B–D) Tumor volume changes in CDX models treated with 7MW4911 or comparators: LS513 (B), LS1034 (C), and AsPC-1 (D). Treatments included 7MW4911, Mab0727(MMAE), 07-0663-h7(MMAE), 07-0663-h7(MF-6), or controls. Data are represented as mean ± SEM ($n = 5$). Data were analyzed using one-way ANOVA.

(legend continued on next page)

Superior *in vivo* efficacy of 7MW4911 in MDR models

GI cancers, particularly CRC, often develop MDR due to repeated exposure to standard chemotherapeutics such as fluoropyrimidines, oxaliplatin, and irinotecan. A major mechanism underlying this resistance is the upregulation of ATP-binding cassette (ABC) transporters, including P-glycoprotein (P-gp/MDR1/ABCB1), MRP1/ABCC1, MRP2/ABCC2, and BCRP/ABCG2, which are frequently enriched in cancer stem-like cells (CSCs). These transporters actively efflux chemotherapeutic agents, reducing intracellular drug concentrations and ultimately impairing therapeutic efficacy.[34–37] MF-6, a topoisomerase I inhibitor that is not a substrate of P-gp, is hypothesized to demonstrate superior efficacy in MDR models compared to MMAE and Deruxtecan (Dxd), which are susceptible to P-gp-mediated efflux.[38–40] This mechanistic distinction positions MF-6 as a promising payload for circumventing transporter-mediated resistance. Initial studies in CRC CDX models demonstrated that 7MW4911 significantly outperformed both Mab0727(MMAE) and 07-0663-h7(MMAE) (WO2023107558A1, University of California, Los Angeles) in the LS513 and LS1034 models (Figure 5A). In the LS513 model, 7MW4911 achieved 82% TGI compared to 52% with Mab0727(MMAE) (Figures 5B and S8U). A similar trend was observed in the LS1034 model, with results confirmed by tumor weight analysis (Figures 5C and S8V). Notably, replacing MMAE with MF-6 in 07-0663-h7(MF-6) also improved efficacy, further validating the contribution of the payload in overcoming resistance (Figures 5B and 5C). In the AsPC-1 pancreatic CDX model, which exhibited a limited response to 07-0663-h7(MMAE) (TGI: 20%), 7MW4911 showed robust anti-tumor activity with 81% TGI. Although 07-0663-h7(MF-6) provided some benefit (TGI: 51%), 7MW4911 demonstrated a substantially greater response, underscoring its superior therapeutic profile in resistant settings (Figures 5D and S8W). To investigate the molecular basis for this enhanced efficacy, we analyzed the expression of ABC transporters in these models. Flow cytometry and IHC analyses confirmed elevated expression of P-gp, MRP1, MRP2, and ABCG2 in both AsPC-1 and CRC models, highlighting an efflux-driven resistance phenotype (Figures S9A–S9E). These findings support the hypothesis that 7MW4911 can bypass efflux transporter-mediated resistance, contributing to its potent *in vivo* efficacy.

Encouraged by these results, we expanded our evaluation to a panel of CRC PDX models. In PDX-CRC-015, a single 10 mg/kg dose of 7MW4911 resulted in 87% TGI, compared to 54% with 07-0663-h7(MMAE) (Figure 5E). Similarly, in PDX-CRC-016, 7MW4911 achieved 94% TGI by day 32, outperforming the 74% TGI observed with 07-0663-h7(MMAE) (Figure 5F). In contrast, both CDH17-targeted ADCs showed comparable efficacy in PDX-CRC-030, reinforcing the potential of CDH17-directed therapies (Figure 5G). Tumor volume and weight measurements corroborated these findings (Figures S8C–S8E and S8M–S8O). Notably, IHC analysis revealed differential expression patterns of ABC transporters across the PDX models. PDX-CRC-015 and PDX-CRC-016 exhibited positive P-gp expression, whereas PDX-CRC-030 showed minimal to undetectable levels. In contrast, the expression of MRP1 and ABCG2 was comparable among all three models, suggesting that P-gp may play a predominant role in mediating drug resistance in this context (Figure S9E). The superior performance of 7MW4911 in transporter-positive models highlights its advantage in overcoming efflux-mediated resistance, a limitation of MMAE-conjugated ADCs. To further validate its efficacy in MDR settings, we established MMAE-resistant CRC models. In the MMAE-resistant LS513 model, 7MW4911 restored anti-tumor activity in mice pre-treated with 07-0663-h7(MMAE), achieving 52% TGI compared to only 21% TGI with continued 07-0663-h7(MMAE) monotherapy (Figure 5H). Similarly, in the MMAE-resistant NCI-H716 model, 7MW4911 achieved 63% TGI, significantly reversing the lack of response seen with Mab0727(MMAE), which showed minimal efficacy (TGI: 5%) (Figure 5I). Remarkably, complete tumor regression was observed in one mouse by day 28, and continued tumor shrinkage was seen in the remaining treated animals throughout the study (Figure 5I). These results underscore the capacity of 7MW4911 to overcome resistance to MMAE-based therapies and highlight its therapeutic potential in MDR CRC, particularly in tumors with high ABC transporter expression or other resistance mechanisms.

Moreover, MF-6 demonstrated superior cytotoxicity compared to other topoisomerase I inhibitors, including SN-38 and DXd, across a panel of GI cancer cell lines (Figure S10). Building on these findings, we evaluated the *in vivo* efficacy of 7MW4911 relative to a CDH17-targeted DXd-based ADC, Mab0727-GGFG-DXd (DAR 4). In the NCI-H508 model, 7MW4911 achieved significantly greater TGI than Mab0727-GGFG-DXd, with 89% vs. 64% TGI, respectively, supported by tumor weight measurements (Figures 5J and S8X). Similarly, in the NCI-H716 model, 7MW4911 yielded 78% TGI compared to 55% with Mab0727-GGFG-DXd, and notably, two mice remained tumor free at day 28 following 7MW4911 treatment (Figure 5K). Together, these results underscore the superior anti-tumor efficacy of 7MW4911 over the DXd-based comparator, supporting MF-6 as a potent payload for advancing CDH17-targeted ADCs in the treatment of GI cancers.

Collectively, these results establish 7MW4911 as a potent CDH17-targeted ADC that outperforms MMAE- and DXd-conjugated counterparts, particularly in ABC transporter-positive, drug-resistant GI cancer models. Its ability to circumvent

(E–G) Tumor volume changes in CRC PDX models treated with 7MW4911, 07-0663-h7(MMAE), or vehicle: PDX-CRC-015 (E), PDX-CRC-016 (F), and PDX-CRC-030 (G). Data are represented as mean ± SEM ($n = 6$). Data were analyzed using one-way ANOVA.
(H and I) *In vivo* efficacy in MMAE-resistant LS513 (H) and NCI-H716 (I) CDX models. Mice were pretreated with 07-0663-h7(MMAE) or Mab0727(MMAE), then received 7MW4911 or continued MMAE treatment. Data are represented as mean ± SEM ($n = 3–6$). Data were analyzed using one-way ANOVA.
(J and K) Tumor volume progression in NCI-H508 (J; 5 mg/kg) and NCI-H716 (K; 10 mg/kg) CDX models following 7MW4911, Mab0727-GGFG-DXd (DAR 4), or vehicle. Data are represented as mean ± SEM ($n = 4–5$).
Statistical analysis was performed using one-way ANOVA. CR, complete regression. ns, not significant; $^{*}p < 0.05$, $^{**}p < 0.01$, $^{***}p < 0.001$, and $^{****}p < 0.0001$. See also Figures S8–S10.

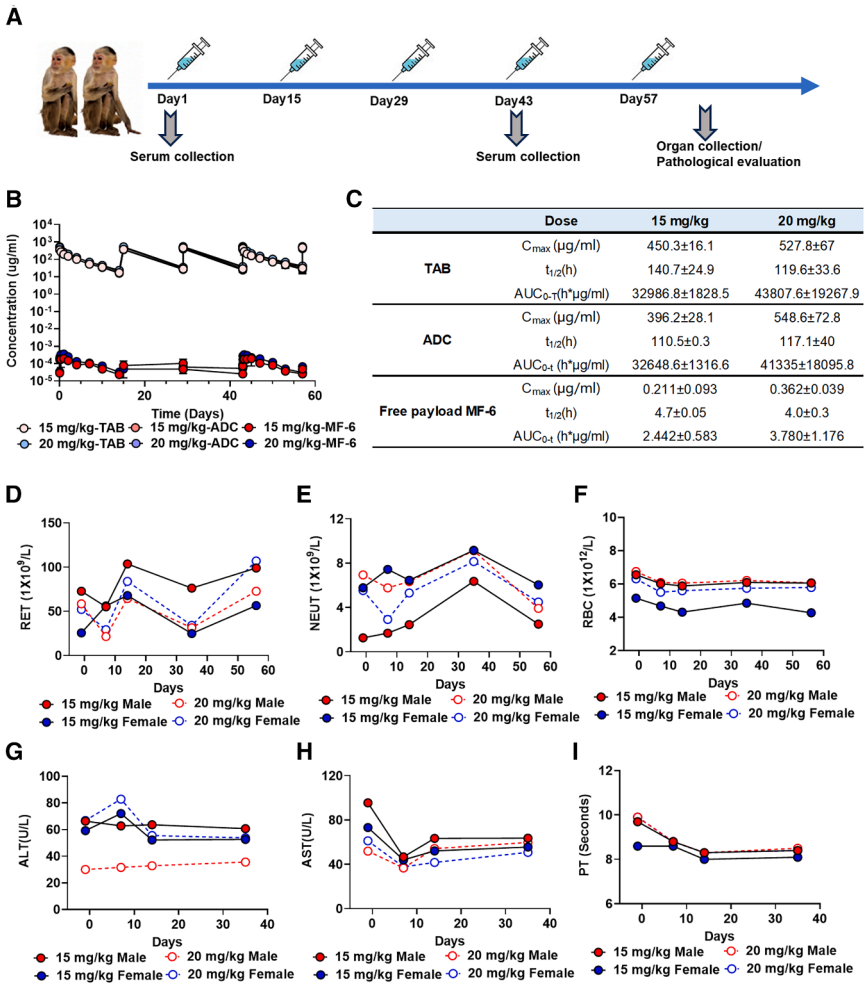

	Dose	15 mg/kg	20 mg/kg
TAB	C_{max} (μg/ml)	450.3±16.1	527.8±67
	$t_{1/2}$(h)	140.7±24.9	119.6±33.6
	AUC_{0-t}(h*μg/ml)	32986.8±1828.5	43807.6±19267.9
ADC	C_{max} (μg/ml)	396.2±28.1	548.6±72.8
	$t_{1/2}$(h)	110.5±0.3	117.1±40
	AUC_{0-t} (h*μg/ml)	32648.6±1316.6	41335±18095.8
Free payload MF-6	C_{max} (μg/ml)	0.211±0.093	0.362±0.039
	$t_{1/2}$(h)	4.7±0.05	4.0±0.3
	AUC_{0-t} (h*μg/ml)	2.442±0.583	3.780±1.176

Figure 6. Nonclinical safety and PK assessment of 7MW4911 in cynomolgus monkeys

(A) Dosing regimen: cynomolgus monkeys (n = 2/group; 1 male and 1 female) received 15 or 20 mg/kg 7MW4911 intravenously every 2 weeks for 8 weeks (days 1, 15, 29, 43, and 57). Clinical observations, pathology, and blood sampling for pharmacokinetic (PK) and clinical assessments were conducted throughout. Necropsy was performed 1 week post-final dose.

(B) PK profiles of TAB, intact ADC, and MF-6 were evaluated over time. Data are represented as mean ± SEM.

(C) Toxicokinetic analysis following repeat dosing assessed systemic exposure and drug accumulation.

(D–F) Hematology parameters. Hematological assessments, including red and white blood cell counts and reticulocyte levels, were monitored for hematologic toxicity.

(G and H) Serum chemistry: liver and kidney function markers were analyzed for organ toxicity.

(I) Coagulation: prothrombin time (PT) and related parameters were assessed for effects on hemostasis.

See also Figure S11.

efflux-mediated resistance highlights its potential as a next-generation therapeutic for treatment-refractory CRC. Further clinical development is warranted to explore its long-term efficacy, safety, and potential in combination regimens targeting multidrug-resistant malignancies.

Favorable safety and toxicokinetic profiles of 7MW4911 in cynomolgus monkeys

To advance the development of 7MW4911 for potential clinical trials in GI cancers, a safety and toxicokinetic evaluation of 7MW4911 was conducted in cynomolgus monkeys, a species known to cross-react with Mab0727. The study involved repeated intravenous dosing, with five doses administered biweekly at 15 and 20 mg/kg, using one male and one female per dose group (Figure 6A). Blood samples were collected during the first and fourth dosing cycles for toxicokinetic analysis and prior to each injection for immunogenicity assessment. Serum concentrations of conjugated antibodies and TABs were quantified using ELISA, while free MF-6 concentrations were measured by LC-tandem mass spectrometry (LC-MS/MS) (Figure 6B). Pharmacokinetic parameters, including C_{max}, $t_{1/2}$, and area under the concentration–time curve from time zero to time t (AUC_{0-t}), were calculated for conjugated antibodies, TABs, and free MF-6 (Figure 6C).

No significant abnormalities were observed in daily activity, ophthalmologic assessments, body weight, body temperature, or food consumption. Additionally, no anti-drug antibodies (ADAs) were detected in any of the samples. At the 20 mg/kg dose, a pigmentary alteration (dark discoloration) of the skin on the right hindlimb was observed in the female animal from day 30 until the study's conclusion. Occasional soft feces were noted in the female animal at 15 mg/kg on day 8 and in the male animal at 20 mg/kg on day 28; however, these were considered unrelated to 7MW4911 as they occurred either during the pre-dose period and were transient, or were infrequent. Decreased reticulocyte (RET) counts were observed in both male and female animals at the 20 mg/kg dose following the first and third doses, compared to pre-dose levels (Figure 6D). No significant changes were noted in other hematological or serum chemistry parameters (Figures 6E–6I and S11A–S11I). At necropsy, a focal black discoloration of the skin on the right hindlimb was observed in the female animal at the 20 mg/kg dose, with no other gross abnormalities identified in the remaining animals. Based on these findings, the highest non-severely toxic dose (HNSTD) of 7MW4911 in cynomolgus monkeys was determined to be 20 mg/kg.

DISCUSSION

ADCs have emerged as a promising therapeutic modality, offering selective delivery of cytotoxic agents to tumor cells while

minimizing systemic toxicity. However, their clinical efficacy in GI cancers has been suboptimal, highlighting the need for emerging targets and optimized therapeutic strategies. In this study, we employed a multi-omics approach to identify potential ADC targets in GI cancers, with a particular emphasis on CRC. Given the critical role of membrane proteins in ADC development, we prioritized the analysis of upregulated cell surface proteins using previously established GESP (genes encoding surface proteins) candidate datasets.[41] Among these, CDH17 emerged as a promising ADC target due to its elevated expression in GI malignancies, especially colorectal and gastric cancers, while exhibiting limited expression in normal tissues, thereby supporting its therapeutic relevance and potential safety profile. Our analysis of TCGA data revealed no significant correlation between CDH17 expression levels and patient survival outcomes in COAD, READ, or stomach adenocarcinoma (STAD). However, differential CDH17 expression was observed in COAD and READ tumors compared to matched normal tissues, as confirmed by RNA-seq data from TCGA and GTEx datasets. While concerns remain regarding potential on-target, off-tumor toxicities due to CDH17 expression in normal tissues, preclinical studies have demonstrated that CDH17-targeted chimeric antigen receptor (CAR)-T cells can effectively eliminate tumors without damaging normal tissues.[32] Furthermore, the basolateral localization of CDH17 in GI epithelial cells restricts its accessibility to ADCs, providing a natural safeguard against toxicity in normal intestinal tissues. Although preliminary evaluations of CDH17-targeted ADCs suggest an acceptable safety profile, comprehensive long-term studies are necessary to fully assess their clinical viability.

A critical consideration in ADC therapy is the bystander effect, wherein the cytotoxic payload not only eliminates antigen-positive tumor cells but also impacts neighboring cells within the tumor microenvironment. In the case of 7MW4911, this effect is primarily driven by the strong hydrophobicity of the MF-6 payload, which facilitates diffusion across cell membranes. While the bystander effect can enhance anti-tumor activity by eradicating heterogeneous tumor cell populations, it also raises concerns regarding potential toxicity in adjacent normal tissues. To mitigate this risk, optimizing cleavable linker designs could enable more controlled payload release, minimizing off-target exposure while preserving therapeutic efficacy. Further investigations are warranted to refine these strategies and ensure a favorable balance between safety and anti-tumor potency for the successful clinical translation of CDH17-targeted ADCs.

Both linker-payload stability and antibody-linker conjugation are critical determinants of ADC performance. Instability can result in premature payload release and systemic toxicity, while excessive stability may prolong circulation time, increasing the risk of off-target effects such as ocular or cardiac toxicity.[42] Our study demonstrated that 7MW4911 exhibits high stability, with 90% of the intact ADC remaining after 240 h in cynomolgus monkey plasma. While this stability ensures effective tumor targeting and payload integrity, it also raises concerns regarding prolonged systemic exposure and potential toxicity. Future pharmacokinetic and biodistribution studies are necessary to comprehensively assess the safety and efficacy of 7MW4911. Additionally, further optimization of ADC design and selectivity is being explored to mitigate these risks.

CRC, the third most common cancer worldwide, presents significant treatment challenges due to its heterogeneity, which complicates therapeutic optimization and limits patient outcomes. Drug resistance remains a major barrier, particularly as the incidence of mCRC continues to rise. A deeper understanding of both intrinsic and acquired resistance mechanisms is critical for the development of more effective treatments. Resistance in CRC is multifactorial, involving genetic mutations, tumor heterogeneity, epithelial-mesenchymal transition (EMT), and the tumor microenvironment. Overexpression of ABC transporters facilitates the efflux of chemotherapeutic agents, reducing intracellular drug accumulation and diminishing treatment efficacy.[43–45] MMAE is a potent tubulin inhibitor widely employed in ADCs, including several FDA-approved therapies. However, its efficacy can be limited by MDR, particularly in GI cancers. Key resistance mechanisms include overexpression of ABC transporters such as P-gp, impaired internalization, altered trafficking, and tubulin modifications.[35,40] Elevated P-gp expression has been frequently observed in chemo-resistant colorectal and gastric tumors, leading to reduced intracellular MMAE retention. Preclinical models confirm that repeated MMAE exposure can induce resistance. Addressing MMAE resistance is therefore critical for enhancing ADC effectiveness in GI malignancies.[46–48] Our studies with MF-6, a topoisomerase I inhibitor, have demonstrated potent cytotoxic activity in CRC cell lines, including those with high ABC transporter expression, suggesting that MF-6 may be more effective than MMAE in overcoming drug resistance. Additionally, MF-6 exhibits greater DNA topoisomerase I inhibition and cytotoxicity compared to DXd, further supporting its potential as an optimized payload for ADC development (Figure S10).[49] Preclinical data indicate that 7MW4911, a CDH17-targeted ADC conjugated to MF-6, exhibits potent anti-tumor activity, including in models resistant to MMAE- and DXd-based therapies. These findings support its potential to overcome drug resistance and warrant further clinical evaluation in CRC.

Understanding the molecular characteristics of CRC is essential for the development of precision therapies. The CMS classification of CRC (CMS1–4) provides insights into tumor heterogeneity and informs potential therapeutic strategies.[50] Our study evaluated the efficacy of 7MW4911 in PDX models representing all four CMS subtypes. Although CDH17 is involved in Wnt/β-catenin signaling in CMS2 tumors, no statistically significant differences in TGI were observed across CMS subtypes. However, larger-scale studies are needed to confirm these findings. Future phase 1 clinical trials will assess 7MW4911 across CMS subtypes to optimize its clinical application. Given the molecular heterogeneity of CRC, combining CDH17-targeted ADCs with existing therapies may enhance efficacy by addressing multiple tumor survival pathways. In CMS1 tumors, which are characterized by high immune checkpoint molecule expression, combining CDH17-targeted ADCs with immune checkpoint inhibitors (ICIs), such as PD-1 or CTLA-4 inhibitors, could enhance anti-tumor immunity. ADCs conjugated to MF-6, such as TS-L6 (trastuzumab-MF-6), have demonstrated the ability to target tumor cells while reactivating immune responses, a strategy that

could be leveraged to overcome the immunosuppressive tumor microenvironment in CRC.[49] In CMS2 tumors, where epidermal growth factor receptor (EGFR) ligand overexpression drives tumor progression, combining CDH17-targeted ADCs with anti-EGFR therapies, such as cetuximab or panitumumab, may offer synergistic benefits. While anti-EGFR agents have shown efficacy in KRAS wild-type tumors, resistance frequently emerges due to acquired KRAS or NRAS mutations.[51–53] Additionally, HER2 amplification has been identified as a key resistance mechanism in CRC.[54] Dual HER2 inhibition with pertuzumab and trastuzumab has demonstrated efficacy in HER2-amplified mCRC, suggesting that integrating these agents with CDH17-targeted ADCs may offer a complementary approach in CMS2 tumors with co-activated EGFR and HER2 pathways.[55] In CMS3 tumors, which are characterized by metabolic dysregulation and frequent KRAS mutations, direct KRAS inhibition represents a promising strategy.[56] The development of KRAS G12C inhibitors provides an avenue for treatment, and their combination with CDH17-targeted ADCs may enhance tumor control.[57] Finally, CMS4 colorectal tumors—marked by mesenchymal features, TGF-β activation, and aberrant angiogenesis—present significant barriers to drug delivery due to dense stroma and abnormal vasculature. Combining CDH17-targeted ADCs like 7MW4911 with vascular normalization agents, such as vascular endothelial growth factor (VEGF) inhibitors (e.g., bevacizumab), may improve therapeutic efficacy by enhancing tumor perfusion and ADC penetration.[58–60] This strategy is particularly relevant for the CMS4 subtype, which is associated with poor prognosis and resistance to standard therapies. While direct studies on these combination strategies remain limited, preclinical and clinical evidence support their potential. Further research is required to optimize these regimens and validate their clinical utility.

In conclusion, CDH17-targeted ADCs, such as 7MW4911, represent a promising advancement in GI cancer treatment. By leveraging CDH17's selective expression in tumors, these therapies have the potential to address critical unmet clinical needs. However, rigorous safety evaluations and long-term studies remain essential to fully assess their clinical viability. Future research should focus on optimizing combination strategies and refining ADC design to maximize therapeutic benefit while minimizing toxicity. Ultimately, robust clinical validation will be critical to ensure the successful translation of these therapies into clinical practice, thereby improving outcomes for patients with GI cancers.

Limitations of the study

CDH17 is primarily localized to the basolateral membrane of normal GI epithelial cells, raising concerns about on-target, off-tumor toxicity. Adverse effects such as mucositis and diarrhea may narrow the therapeutic window and present challenges for safe clinical application. A major limitation is the absence of preclinical models that accurately replicate human CDH17 expression and associated toxicities, hindering reliable safety and efficacy predictions during early drug development.

Our efficacy assessments relied on PDX models, which retain tumor heterogeneity but do not capture the native tumor microenvironment or metastatic behavior of CRC. This limits insight into therapeutic performance under physiologically relevant conditions. Future studies incorporating orthotopic, metastatic, or genetically engineered mouse models (GEMMs) are warranted to better characterize efficacy and safety.

The lack of predictive biomarkers for CDH17 expression further complicates patient selection and may impede the identification of individuals most likely to benefit. Due to limited model availability, our study could not support statistical comparisons across CMS or between microsatellite stability subtypes (microsatellite stable [MSS] vs. microsatellite instability high [MSI-H]), as all available models with known status were MSS.

Finally, while the current study focused on monotherapy, combinatorial strategies—such as co-targeting EGFR or immune checkpoints—may enhance efficacy and warrant future investigation. Addressing these limitations through improved modeling, biomarker development, and combination approaches will be critical for advancing CDH17-targeting ADCs toward clinical application.

RESOURCE AVAILABILITY

Lead contact

Further information and requests for resources and reagents should be directed to and will be fulfilled by the lead contact, Xun Gui (xun.gui@mabwell.com).

Materials availability

All materials generated in this study are availability through the lead contact.

Data and code availability

- All data reported in this paper will be shared by the lead contact upon request.
- This paper does not report original code.
- Any additional information required to reanalyze the data reported in this paper is available from the lead contact upon request.

ACKNOWLEDGMENTS

This work was supported by Mabwell (Shanghai) Bioscience Co., Ltd. We gratefully acknowledge the support provided by colleagues at Mabwell (Shanghai) Bioscience Co., Ltd., and Jiangsu Mabwell Health Pharmaceutical R&D Co., Ltd.

AUTHOR CONTRIBUTIONS

Study initiation, D.L., H.W., X.T., and X.G.; supervision, D.L.; research activity supervision, H.W., X.T., and X.G.; project direction, X.G.; writing – original draft, Rui Wang; writing – review & editing, X.G. and P.F.; experiment design, Rui Wang and P.F.; data curation, Rui Wang; data analysis, P.F., X.C., J.J., and W.P.; study design, X.C.; data generation, X.C.; experimental work, J.J. and W.P.; bioinformatic analysis, J.W. and C.G.; ADC conjugation and characterization assays, F.M., W.Z., and Z.W.; toxicology study direction, D.Y.; *in vivo* model data support, Rongjuan Wang.

DECLARATION OF INTERESTS

All authors are employees of Mabwell (Shanghai) Bioscience Co., Ltd., or Jiangsu Mabwell Health Pharmaceutical R&D Co., Ltd., and may hold shares in Mabwell (Shanghai) Bioscience Co., Ltd. Rui Wang, P.F., W.Z., X.T., X.G., and D.L. are listed as inventors on a patent application for the anti-CDH17 ADC 7MW4911.

STAR★METHODS

Detailed methods are provided in the online version of this paper and include the following:

- KEY RESOURCES TABLE
- EXPERIMENTAL MODEL AND STUDY PARTICIPANT DETAILS
  - Cell lines
  - Xenograft models
  - Tissue distribution in tumor-bearing mice
  - Non-human primate studies
- METHOD DETAILS
  - Antibodies
  - ELISA
  - Flow cytometry
  - IHC analysis
  - Bio layer interferometry
  - Development of Mab0727
  - Hydrophobicity evaluation by HIC-HPLC
  - Thermal stability assessment
  - ADC preparation
  - ADC concentration and DAR measurement
  - ε: Extinction coefficients
  - ADC aggregation measurement
  - Cell internalization assay
  - Cell cytotoxicity assay
  - PK of 7MW4911 in BALB/c mice
  - *In vitro* stability of 7MW4911 in monkey plasma
  - Bystander effect
  - Total antibody bioanalytical assay
  - Conjugated antibody bioanalytical assay
  - Analytical assay for free MF-6 quantification
- QUANTIFICATION AND STATISTICAL ANALYSIS

SUPPLEMENTAL INFORMATION

Supplemental information can be found online at https://doi.org/10.1016/j.xcrm.2025.102213.

Received: December 17, 2024
Revised: April 12, 2025
Accepted: June 3, 2025
Published: July 1, 2025

REFERENCES

1. Bray, F., Laversanne, M., Sung, H., Ferlay, J., Siegel, R.L., Soerjomataram, I., and Jemal, A. (2024). Global cancer statistics 2022: GLOBOCAN estimates of incidence and mortality worldwide for 36 cancers in 185 countries. CA Cancer J. Clin. *74*, 229–263. https://doi.org/10.3322/caac.21834.

2. Baraniskin, A., Van Laethem, J.-L., Wyrwicz, L., Guller, U., Wasan, H.S., Matysiak-Budnik, T., Gruenberger, T., Ducreux, M., Carneiro, F., Van Cutsem, E., et al. (2017). Clinical relevance of molecular diagnostics in gastrointestinal (GI) cancer: European Society of Digestive Oncology (ESDO) expert discussion and recommendations from the 17th European Society for Medical Oncology (ESMO)/World Congress on Gastrointestinal Cancer, Barcelona. Eur. J. Cancer *86*, 305–317. https://doi.org/10.1016/j.ejca.2017.09.021.

3. Sonnenberg, W.R. (2017). Gastrointestinal Malignancies. Prim. Care *44*, 721–732. https://doi.org/10.1016/j.pop.2017.07.013.

4. Diaz, L.A., and Le, D.T. (2015). PD-1 Blockade in Tumors with Mismatch-Repair Deficiency. N. Engl. J. Med. *373*, 1979. https://doi.org/10.1056/NEJMc1510353.

5. Baah, S., Laws, M., and Rahman, K.M. (2021). Antibody–Drug Conjugates—A Tutorial Review. Molecules (Basel) *26*, 2943. https://doi.org/10.3390/molecules26102943.

6. Criscitiello, C., Morganti, S., and Curigliano, G. (2021). Antibody-drug conjugates in solid tumors: a look into novel targets. J. Hematol. Oncol. *14*, 20. https://doi.org/10.1186/s13045-021-01035-z.

7. Hafeez, U., Parakh, S., Gan, H.K., and Scott, A.M. (2020). Antibody–Drug Conjugates for Cancer Therapy. Molecules (Basel) *25*, 4764. https://doi.org/10.3390/molecules25204764.

8. Molinelli, C., Parisi, F., Razeti, M.G., Arecco, L., Cosso, M., Fregatti, P., Del Mastro, L., Poggio, F., and Lambertini, M. (2021). Trastuzumab emtansine (T-DM1) as adjuvant treatment of HER2-positive early breast cancer: safety and efficacy. Expert Rev. Anticancer Ther. *21*, 241–250. https://doi.org/10.1080/14737140.2021.1857243.

9. Modi, S., Saura, C., Yamashita, T., Park, Y.H., Kim, S.-B., Tamura, K., Andre, F., Iwata, H., Ito, Y., Tsurutani, J., et al. (2020). Trastuzumab Deruxtecan in Previously Treated HER2-Positive Breast Cancer. N. Engl. J. Med. *382*, 610–621. https://doi.org/10.1056/NEJMoa1914510.

10. Modi, S., Park, H., Murthy, R.K., Iwata, H., Tamura, K., Tsurutani, J., Moreno-Aspitia, A., Doi, T., Sagara, Y., Redfern, C., et al. (2020). Antitumor Activity and Safety of Trastuzumab Deruxtecan in Patients With HER2-Low-Expressing Advanced Breast Cancer: Results From a Phase Ib Study. J. Clin. Oncol. *38*, 1887–1896. https://doi.org/10.1200/JCO.19.02318.

11. Riccardi, F., Dal Bo, M., Macor, P., and Toffoli, G. (2023). A comprehensive overview on antibody-drug conjugates: from the conceptualization to cancer therapy. Front. Pharmacol. *14*, 1274088. https://doi.org/10.3389/fphar.2023.1274088.

12. Drago, J.Z., Modi, S., and Chandarlapaty, S. (2021). Unlocking the potential of antibody-drug conjugates for cancer therapy. Nat. Rev. Clin. Oncol. *18*, 327–344. https://doi.org/10.1038/s41571-021-00470-8.

13. Joubert, N., Beck, A., Dumontet, C., and Denevault-Sabourin, C. (2020). Antibody-Drug Conjugates: The Last Decade. Pharmaceuticals *13*, 245. https://doi.org/10.3390/ph13090245.

14. Dumontet, C., Reichert, J.M., Senter, P.D., Lambert, J.M., and Beck, A. (2023). Antibody-drug conjugates come of age in oncology. Nat. Rev. Drug Discov. *22*, 641–661. https://doi.org/10.1038/s41573-023-00709-2.

15. Raghav, K., Siena, S., Takashima, A., Kato, T., Van den Eynde, M., Pietrantonio, F., Komatsu, Y., Kawakami, H., Peeters, M., Andre, T., et al. (2024). Trastuzumab deruxtecan in patients with HER2-positive advanced colorectal cancer (DESTINY-CRC02): primary results from a multicentre, randomised, phase 2 trial. Lancet Oncol. *25*, 1147–1162. https://doi.org/10.1016/S1470-2045(24)00380-2.

16. Ahcene Djaballah, S., Daniel, F., Milani, A., Ricagno, G., and Lonardi, S. (2022). HER2 in Colorectal Cancer: The Long and Winding Road From Negative Predictive Factor to Positive Actionable Target. Am. Soc. Clin. Oncol. Educ. Book. *42*, 1–14. https://doi.org/10.1200/EDBK_351354.

17. Gessner, R., and Tauber, R. (2000). Intestinal Cell Adhesion Molecules: Liver-Intestine Cadherin. Ann. N. Y. Acad. Sci. *915*, 136–143. https://doi.org/10.1111/j.1749-6632.2000.tb05236.x.

18. Dantzig, A.H., Hoskins, J.A., Tabas, L.B., Bright, S., Shepard, R.L., Jenkins, I.L., Duckworth, D.C., Sportsman, J.R., Mackensen, D., and Rosteck, P.R. (1994). Association of intestinal peptide transport with a protein related to the cadherin superfamily. Science *264*, 430–433. https://doi.org/10.1126/science.8153632.

19. Baumgartner, W. (2013). Possible roles of LI-Cadherin in the formation and maintenance of the intestinal epithelial barrier. Tissue Barriers *1*, e23815. https://doi.org/10.4161/tisb.23815.

20. Takamura, M., Yamagiwa, S., Matsuda, Y., Ichida, T., and Aoyagi, Y. (2013). Involvement of liver-intestine cadherin in cancer progression. Med. Mol. Morphol. *46*, 1–7. https://doi.org/10.1007/s00795-012-0003-y.

21. Ko, S., Chu, K.-M., Luk, J.M., Wong, B.W., Yuen, S.-T., Leung, S.-Y., and Wong, J. (2004). Overexpression of LI-cadherin in gastric cancer is

associated with lymph node metastasis. Biochem. Biophys. Res. Commun. *319*, 562–568. https://doi.org/10.1016/j.bbrc.2004.04.197.

22. Zheng, B.-H., Shen, S., Wong, K.-F., Gong, Z.-J., Sun, W.-T., Ni, X.-J., Wang, J.-W., Hu, M.-Y., Liu, H., Ni, X.-L., et al. (2021). Clinical correlation of cadherin-17 marker with advanced tumor stages and poor prognosis of cholangiocarcinoma. J. Surg. Oncol. *123*, 1253–1262. https://doi.org/10.1002/jso.26399.
23. Liu, L.X., Lee, N.P., Chan, V.W., Xue, W., Zender, L., Zhang, C., Mao, M., Dai, H., Wang, X.L., Xu, M.Z., et al. (2009). Targeting cadherin-17 inactivates Wnt signaling and inhibits tumor growth in liver carcinoma. Hepatology (Baltim., Md.) *50*, 1453–1463. https://doi.org/10.1002/hep.23143.
24. Lin, Z., Zhang, C., Zhang, M., Xu, D., Fang, Y., Zhou, Z., Chen, X., Qin, N., and Zhang, X. (2014). Targeting Cadherin-17 Inactivates Ras/Raf/MEK/ERK Signaling and Inhibits Cell Proliferation in Gastric Cancer. PLoS One *9*, e85296. https://doi.org/10.1371/journal.pone.0085296.
25. Bartolomé, R.A., Barderas, R., Torres, S., Fernandez-Aceñero, M.J., Mendes, M., García-Foncillas, J., Lopez-Lucendo, M., and Casal, J.I. (2014). Cadherin-17 interacts with α2β1 integrin to regulate cell proliferation and adhesion in colorectal cancer cells causing liver metastasis. Oncogene *33*, 1658–1669. https://doi.org/10.1038/onc.2013.117.
26. Lee, N.P., Poon, R.T.P., Shek, F.H., Ng, I.O.L., and Luk, J.M. (2010). Role of cadherin-17 in oncogenesis and potential therapeutic implications in hepatocellular carcinoma. Biochim. Biophys. Acta *1806*, 138–145. https://doi.org/10.1016/j.bbcan.2010.05.002.
27. Chan, K., Tung, L., Lam, H., Choi, M., Wong, M., Fatima, S., Tam, P., Wang, H., Liu, E., Bian, Z., and Lee, N. (2016). Survival Benefit of a Monoclonal Antibody against Cadherin-17 in an Orthotopic Liver Tumor Xenograft Model. JALSI *4*, 1–10. https://doi.org/10.9734/JALSI/2016/22188.
28. Xu, Y., Zhang, J., Liu, Q.-S., and Dong, W.-G. (2012). Knockdown of liver-intestine cadherin decreases BGC823 cell invasiveness and metastasis in vivo. World J. Gastroenterol. *18*, 3129–3137. https://doi.org/10.3748/wjg.v18.i24.3129.
29. Panarelli, N.C., Yantiss, R.K., Yeh, M.M., Liu, Y., and Chen, Y.-T. (2012). Tissue-Specific Cadherin CDH17 Is a Useful Marker of Gastrointestinal Adenocarcinomas With Higher Sensitivity Than CDX2. Am. J. Clin. Pathol. *138*, 211–222. https://doi.org/10.1309/AJCPKSHXI3XEHW1J.
30. Wong, K.K. (2023). Integrated transcriptomics and proteomics data analysis identifies CDH17 as a key cell surface target in colorectal cancer. Comput. Biol. Chem. *105*, 107897. https://doi.org/10.1016/j.compbiolchem.2023.107897.
31. García-Martínez, J.M., Wang, S., Weishaeupl, C., Wernitznig, A., Chetta, P., Pinto, C., Ho, J., Dutcher, D., Gorman, P.N., Kroe-Barrett, R., et al. (2021). Selective Tumor Cell Apoptosis and Tumor Regression in CDH17-Positive Colorectal Cancer Models using BI 905711, a Novel Liver-Sparing TRAILR2 Agonist. Mol. Cancer Ther. *20*, 96–108. https://doi.org/10.1158/1535-7163.MCT-20-0253.
32. Feng, Z., He, X., Zhang, X., Wu, Y., Xing, B., Knowles, A., Shan, Q., Miller, S., Hojnacki, T., Ma, J., et al. (2022). Potent suppression of neuroendocrine tumors and gastrointestinal cancers by CDH17CAR T cells without toxicity to normal tissues. Nat. Cancer *3*, 581–594. https://doi.org/10.1038/s43018-022-00344-7.
33. Guinney, J., Dienstmann, R., Wang, X., De Reyniès, A., Schlicker, A., Soneson, C., Marisa, L., Roepman, P., Nyamundanda, G., Angelino, P., et al. (2015). The consensus molecular subtypes of colorectal cancer. Nat. Med. *21*, 1350–1356. https://doi.org/10.1038/nm.3967.
34. Begicevic, R.-R., and Falasca, M. (2017). ABC Transporters in Cancer Stem Cells: Beyond Chemoresistance. Int. J. Mol. Sci. *18*, 2362. https://doi.org/10.3390/ijms18112362.
35. Goda, K., Bacsó, Z., and Szabó, G. (2009). Multidrug resistance through the spectacle of P-glycoprotein. Curr. Cancer Drug Targets *9*, 281–297. https://doi.org/10.2174/156800909788166493.
36. Steinbichler, T.B., Dudás, J., Skvortsov, S., Ganswindt, U., Riechelmann, H., and Skvortsova, I.-I. (2018). Therapy resistance mediated by cancer stem cells. Semin. Cancer Biol. *53*, 156–167. https://doi.org/10.1016/j.semcancer.2018.11.006.
37. Fan, J., To, K.K.W., Chen, Z.-S., and Fu, L. (2023). ABC transporters affects tumor immune microenvironment to regulate cancer immunotherapy and multidrug resistance. Drug Resist. Updat. *66*, 100905. https://doi.org/10.1016/j.drup.2022.100905.
38. Liu-Kreyche, P., Shen, H., Marino, A.M., Iyer, R.A., Humphreys, W.G., and Lai, Y. (2019). Lysosomal P-gp-MDR1 Confers Drug Resistance of Brentuximab Vedotin and Its Cytotoxic Payload Monomethyl Auristatin E in Tumor Cells. Front. Pharmacol. *10*, 749. https://doi.org/10.3389/fphar.2019.00749.
39. Cabaud, O., Berger, L., Crompot, E., Adélaide, J., Finetti, P., Garnier, S., Guille, A., Carbuccia, N., Farina, A., Agavnian, E., et al. (2022). Overcoming Resistance to Anti-Nectin-4 Antibody-Drug Conjugate. Mol. Cancer Ther. *21*, 1227–1235. https://doi.org/10.1158/1535-7163.MCT-22-0013.
40. Loo, T.W., and Clarke, D.M. (2005). Recent progress in understanding the mechanism of P-glycoprotein-mediated drug efflux. J. Membr. Biol. *206*, 173–185. https://doi.org/10.1007/s00232-005-0792-1.
41. Hu, Z., Yuan, J., Long, M., Jiang, J., Zhang, Y., Zhang, T., Xu, M., Fan, Y., Tanyi, J.L., Montone, K.T., et al. (2021). The Cancer Surfaceome Atlas integrates genomic, functional and drug response data to identify actionable targets. Nat. Cancer *2*, 1406–1422. https://doi.org/10.1038/s43018-021-00282-w.
42. Colombo, R. (2023). Refining our understanding of ADCs: Drug development insights from 40 years of data..
43. Gottesman, M.M., and Ling, V. (2006). The molecular basis of multidrug resistance in cancer: the early years of P-glycoprotein research. FEBS Lett. *580*, 998–1009. https://doi.org/10.1016/j.febslet.2005.12.060.
44. Du, J., He, Y., Li, P., Wu, W., Chen, Y., and Ruan, H. (2018). IL-8 regulates the doxorubicin resistance of colorectal cancer cells via modulation of multidrug resistance 1 (MDR1). Cancer Chemother. Pharmacol. *81*, 1111–1119. https://doi.org/10.1007/s00280-018-3584-x.
45. Nielsen, D.L., Palshof, J.A., Brünner, N., Stenvang, J., and Viuff, B.M. (2017). Implications of ABCG2 Expression on Irinotecan Treatment of Colorectal Cancer Patients: A Review. Int. J. Mol. Sci. *18*, 1926. https://doi.org/10.3390/ijms18091926.
46. Xu, H.-W., Xu, L., Hao, J.-H., Qin, C.-Y., and Liu, H. (2010). Expression of P-glycoprotein and multidrug resistance-associated protein is associated with multidrug resistance in gastric cancer. J. Int. Med. Res. *38*, 34–42. https://doi.org/10.1177/147323001003800104.
47. Hu, W.-Q., Peng, C.-W., and Li, Y. (2009). The expression and significance of P-glycoprotein, lung resistance protein and multidrug resistance-associated protein in gastric cancer. J. Exp. Clin. Cancer Res. *28*, 144. https://doi.org/10.1186/1756-9966-28-144.
48. Shi, W.-J., and Gao, J.-B. (2016). Molecular mechanisms of chemoresistance in gastric cancer. World J. Gastrointest. Oncol. *8*, 673–681. https://doi.org/10.4251/wjgo.v8.i9.673.
49. Tan, X., Fang, P., Li, K., You, M., Cao, Y., Xu, H., Zhu, X., Wang, L., Wei, X., Wen, H., et al. (2023). A HER2-targeted antibody-novel DNA topoisomerase I inhibitor conjugate induces durable adaptive antitumor immunity by activating dendritic cells. mAbs *15*, 2220466. https://doi.org/10.1080/19420862.2023.2220466.
50. Wang, W., Kandimalla, R., Huang, H., Zhu, L., Li, Y., Gao, F., Goel, A., and Wang, X. (2019). Molecular subtyping of colorectal cancer: Recent progress, new challenges and emerging opportunities. Semin. Cancer Biol. *55*, 37–52. https://doi.org/10.1016/j.semcancer.2018.05.002.
51. Khambata-Ford, S., Garrett, C.R., Meropol, N.J., Basik, M., Harbison, C.T., Wu, S., Wong, T.W., Huang, X., Takimoto, C.H., Godwin, A.K., et al. (2007). Expression of epiregulin and amphiregulin and K-ras mutation status predict disease control in metastatic colorectal cancer patients treated with cetuximab. J. Clin. Oncol. *25*, 3230–3237. https://doi.org/10.1200/JCO.2006.10.5437.

52. Amado, R.G., Wolf, M., Peeters, M., Van Cutsem, E., Siena, S., Freeman, D.J., Juan, T., Sikorski, R., Suggs, S., Radinsky, R., et al. (2023). Wild-Type KRAS Is Required for Panitumumab Efficacy in Patients With Metastatic Colorectal Cancer. J. Clin. Oncol. *41*, 3278–3286. https://doi.org/10.1200/JCO.22.02758.

53. Douillard, J.-Y., Siena, S., Cassidy, J., Tabernero, J., Burkes, R., Barugel, M., Humblet, Y., Bodoky, G., Cunningham, D., Jassem, J., et al. (2010). Randomized, phase III trial of panitumumab with infusional fluorouracil, leucovorin, and oxaliplatin (FOLFOX4) versus FOLFOX4 alone as first-line treatment in patients with previously untreated metastatic colorectal cancer: the PRIME study. J. Clin. Oncol. *28*, 4697–4705. https://doi.org/10.1200/JCO.2009.27.4860.

54. Bertotti, A., Migliardi, G., Galimi, F., Sassi, F., Torti, D., Isella, C., Corà, D., Di Nicolantonio, F., Buscarino, M., Petti, C., et al. (2011). A molecularly annotated platform of patient-derived xenografts ("xenopatients") identifies HER2 as an effective therapeutic target in cetuximab-resistant colorectal cancer. Cancer Discov. *1*, 508–523. https://doi.org/10.1158/2159-8290.CD-11-0109.

55. Meric-Bernstam, F., Hurwitz, H., Raghav, K.P.S., McWilliams, R.R., Fakih, M., VanderWalde, A., Swanton, C., Kurzrock, R., Burris, H., Sweeney, C., et al. (2019). Pertuzumab plus trastuzumab for HER2-amplified metastatic colorectal cancer (MyPathway): an updated report from a multicentre, open-label, phase 2a, multiple basket study. Lancet Oncol. *20*, 518–530. https://doi.org/10.1016/S1470-2045(18)30904-5.

56. Zhu, G., Pei, L., Xia, H., Tang, Q., and Bi, F. (2021). Role of oncogenic KRAS in the prognosis, diagnosis and treatment of colorectal cancer. Mol. Cancer *20*, 143. https://doi.org/10.1186/s12943-021-01441-4.

57. Dhillon, S. (2023). Adagrasib: First Approval. Drugs (Basel) *83*, 275–285. https://doi.org/10.1007/s40265-023-01839-y.

58. Rosen, L.S., Jacobs, I.A., and Burkes, R.L. (2017). Bevacizumab in Colorectal Cancer: Current Role in Treatment and the Potential of Biosimilars. Target. Oncol. *12*, 599–610. https://doi.org/10.1007/s11523-017-0518-1.

59. Oki, E., Makiyama, A., Miyamoto, Y., Kotaka, M., Kawanaka, H., Miwa, K., Kabashima, A., Noguchi, T., Yuge, K., Kashiwada, T., et al. (2021). Trifluridine/tipiracil plus bevacizumab as a first-line treatment for elderly patients with metastatic colorectal cancer (KSCC1602): A multicenter phase II trial. Cancer Med. *10*, 454–461. https://doi.org/10.1002/cam4.3618.

60. Venook, A.P., Niedzwiecki, D., Lenz, H.-J., Innocenti, F., Fruth, B., Meyerhardt, J.A., Schrag, D., Greene, C., O'Neil, B.H., Atkins, J.N., et al. (2017). Effect of First-Line Chemotherapy Combined With Cetuximab or Bevacizumab on Overall Survival in Patients With KRAS Wild-Type Advanced or Metastatic Colorectal Cancer: A Randomized Clinical Trial. JAMA *317*, 2392–2401. https://doi.org/10.1001/jama.2017.7105.

STAR★METHODS

KEY RESOURCES TABLE

REAGENT or RESOURCE	SOURCE	IDENTIFIER
Antibodies		
LI-cadherin antibody (H-1)	Santa Cruz Biotechnology	Cat#sc-393533
Cadherin-17 antibody	Novus Biologicals	Cat#NBP2-79857; RRID: AB_3405596
P Glycoprotein antibody	GeneTex	Cat#GTX42220; RRID: AB_11173104
Anti-P Glycoprotein antibody	Abcam	Cat#ab170904; RRID: AB_2687930
MRP1 antibody	Santa Cruz Biotechnology	Cat#sc-18835; RRID: AB_627964
MRP2 antibody	Santa Cruz Biotechnology	Cat#sc-59611; RRID: AB_631969
Anti-BCRP/ABCG2 antibody [EPR21122]	Abcam	Cat#ab229193
LI cadherin antibody [ERP3996]	Abcam	Cat#ab109190; RRID: AB_10861627
07-0663-h7	WO2023107558	N/A
PTA001-A4	US20160039933A1	N/A
irrelevant IgG	This paper	N/A
Mab0727	This paper	N/A
7MW4911	This paper	N/A
Mab0727(MMAE)	This paper	N/A
07-0663-h7(MMAE)	This paper	N/A
07-0663-h7(MF-6)	This paper	N/A
Anti-MF-6 antibody	This paper	N/A
APC AffiniPure Goat Anti-Human IgG, Fcγ fragment specific	Jackson ImmunoResearch	Cat#109-135-098; RRID: AB_2337690
Peroxidase AffiniPure Goat Anti-Human IgG, Fcγ fragment specific	Jackson ImmunoResearch	Cat#109-035-098; RRID: AB_2337586
Peroxidase-AffiniPure F(ab')2 Fragment Goat Anti-Rat IgG, Fc_ Fragment Specific	Jackson ImmunoResearch	Cat#112-036-071; RRID: AB_2338144
Peroxidase AffiniPure Goat Anti-Rabbit IgG (H + L)	Jackson ImmunoResearch	Cat#111-035-144; RRID: AB_2307391
Biological samples		
Cynomolgus monkey plasma	PharmaLegacy Laboratories	N/A
Human normal and cancer tissue microarrays	Xi'an Zhongke Guanghua Bioaitech Co., Ltd.	N/A
Mouse serum	Shanghai Medsyin Pharmaceutical Technology Co., Ltd.	N/A
ex vivo tumor tissue of CDX models	Yicon BioMedical Technology Inc.	N/A
Chemicals, peptides, and recombinant proteins		
TCEP	Sigma-Aldrich	CAS#51805-45-9
BL20E	Anhui Haoyuan Pharmaceutical Co., Ltd.	N/A
MF-L6	Anhui Haoyuan Pharmaceutical Co., Ltd.	N/A
DMAc	Sigma-Aldrich	CAS#127-19-5
Sodium phosphate Monobasic Monohydrate	Merck	CAS#10049-21-5
Ammonium sulfate	Merck	CAS#7783-20-2
Tetrabutylammonium bromide	Sigma-Aldrich	CAS#1643-19-2
Isopropanol	Sigma-Aldrich	CAS#67-63-0
Methyl *tert*-butyl ether	Sigma-Aldrich	CAS#1634-04-4
Formic acid	Honeywell	CAS#64-18-6
Acetonitrile	Merck	CAS#75-05-8

(*Continued on next page*)

Continued

REAGENT or RESOURCE	SOURCE	IDENTIFIER
Ammonium formate	Sigma-Aldrich	CAS#540-69-2
Versene solution	Gibco™	Cat#15040066
1-Step™ Ultra TMB-ELISA	Thermo scientific	REF#34029
HAT medium supplement(50x) Hybrid-Max®	Sigma Aldrich	Cat#H0262-1VL
PBS (pH7.4)	Shanghai Basalmedia Technologies CO.,Ltd.	REF#B320KL
Human CDH17 protein	Kactusbio Inc.	Cat#CDH-HM117
Cynomolgus CDH17 protein	Kactusbio Inc.	Cat#CDH-CM127
Mouse CDH17 protein	ACROBiosystems	Cat#CA7-M52H5
Rat CDH17 protein	Sino Biological, Inc.	Cat#80283-R08H
Canis CDH17 protein	This paper	N/A
Critical commercial assays		
iQue® Human Antibody Internalization Reagent	Sartorius	Cat#90565
ProteoStat® Thermal Shift Stability Assay Kit	Enzo Life	Cat#ENZ-51027-K400
Bio-Lite Luciferase Assay System reagent	Vazyme	Cat#DD1201-03
Quantitative Analysis Kit (QIFIKIT®)	Agilent Technologies	Cat#K0078
Bond Polymer Refine Detection Kit	Leica	Cat#DS9800
Deposited data		
TCGA/GTEx Gene expression data	UCSC Toil RNA-seq Recompute	https://xenabrowser.net/datapages/?cohort=TCGA%20TARGET%20GTEx&removeHub=https%3A%2F%2Fxena.treehouse.gi.ucsc.edu%3A443
HPA tissue protein expression (IHC)	The Human Protein Atlas	https://www.proteinatlas.org/
single cell RNA-seq dataset for colorectal cancer	GEO	GEO: GSE132465
single cell RNA-seq dataset for gastric cancer	GEO	GEO: GSE163558
Gene Encoding Surface Proteins dataset	Hu et al., 2021[41]	N/A
Gene expression data and protein mutations data	https://yicondatabase.com/index.html	N/A
Gene expression data and protein mutations data	LIDE's PMed-TRIAL PDX Database	N/A
Experimental models: Cell lines		
HEK293-Rhesus CDH17 Cell line	Genomeditech	GM-C25981
Human: SNU-C1	ATCC	CRL-5972; RRID: CVCL_1708
Human: SK-CO-1	ATCC	CBP60038; RRID: CVCL_0626
Human:LS513	ATCC	CBP61154; RRID: CVCL_1386
Human:LS1034	ATCC	CBP60013; RRID: CVCL_1382
Human: NCI-H508	ATCC	CBP60795; RRID: CVCL_1564
Human: NCI-H716	ATCC	CBP60737; RRID: CVCL_1581
Human: HT55	ATCC	CBP60012; RRID: CVCL_A8FJ
Human: CL40	ATCC	CBP60565; RRID: CVCL_1982
Human: DLD-1	ATCC	CBP60037; RRID: CVCL_0248
Human: SNU-16	ATCC	CBP60502; RRID: CVCL_0076
Human: 23132/87	DSMZ	CBP60475; RRID: CVCL_1046
Human: AsPC-1	ATCC	CBP60546; RRID: CVCL_0152

(*Continued on next page*)

Continued

REAGENT or RESOURCE	SOURCE	IDENTIFIER
Experimental models: Organisms/strains		
Female BALB/C mice and SJL mice for animal immunization	SHANGHAI SLAC LABORATORY ANIMAL CO. LTD	N/A
Female BALB/C nude mice for CDX models	Gempharmatech, China	N/A
Female NCG mice for CDX models	Gempharmatech, China	N/A
Female NDG mice for CDX models	Biocytogen pharmaceuticals, China	N/A
PDX-CRC-004	Yicon BioMedical Technology Inc.	N/A
PDX-CRC-007	Yicon BioMedical Technology Inc.	N/A
PDX-CRC-009	Yicon BioMedical Technology Inc.	N/A
PDX-CRC-015	Yicon BioMedical Technology Inc.	N/A
PDX-CRC-016	Yicon BioMedical Technology Inc.	N/A
PDX-CRC-030	Yicon BioMedical Technology Inc.	N/A
PDX-33	Hanjiang Biotechnology	N/A
LD1-2012-362429	LIDE Biotech Co., China	N/A
LD1-2012-200671	LIDE Biotech Co., China	N/A
LD1-0012-360837	LIDE Biotech Co., China	N/A
PDX-STAD-050	Yicon BioMedical Technology Inc.	N/A
LD1-2017-361697	LIDE Biotech Co., China	N/A
LD1-0017-200697	LIDE Biotech Co., China	N/A
Cynomolgus monkeys for toxicity study	Shanghai Institute of Materia Medica, Chinese Academy of Sciences	N/A
Software and algorithms		
GraphPad Prism	https://www.graphpad.com	N/A
Pannoramic Digital Slide Scanner	3DHISTECH, Ltd.	N/A
R v4.2.2	https://www.r-project.org/	N/A
iQue Screener PLUS	Sartorius	N/A

EXPERIMENTAL MODEL AND STUDY PARTICIPANT DETAILS

Cell lines

Human tumor cell lines were obtained from ATCC (via Cobioer, Nanjing, China) or DSMZ, and recombinant rhesus CDH17 cell lines from Genomeditech (Shanghai). All cell lines were authenticated by STR analysis: genomic DNA was extracted using the Axygen kit, PCR amplified with the Promega GenePrint System, and analyzed on an ABI 3730XL Genetic Analyzer; profiles were matched against ATCC, DSMZ, and JCRB databases using GeneMapper 4.0. Mycoplasma testing confirmed all cell lines were negative. Cells were cultured in vendor-recommended media at 37°C with 5% CO_2.

Xenograft models

All *in vivo* procedures were performed in compliance with local guidelines established by the Institutional Animal Care and Use Committee (IACUC) and accredited by the Association for Assessment and Accreditation of Laboratory Animal Care (AAALAC). Human colon cancer cells, gastric cancer cells, or pancreatic cancer cells, as well as 2 mm × 2 mm × 2 mm colorectal cancer tissue fragments, or gastric cancer tissue fragments were inoculated subcutaneously into the right anterior flank of female mice aged 6 to 8 weeks. Once the tumors reached an average volume of approximately 200 mm^3, the mice were randomly divided into treatment groups.

All groups received intravenous injections, administered either as a single dose or as two doses, with Day 0 designated as the day of the first administration. Post-administration, tumor volume and mouse body weight were measured biweekly, and the relationships between weight changes over time and tumor volume changes over time were recorded. At the end of the experiment, the tumor-bearing mice were euthanized, and the tumors from both control and treatment groups were excised for photographic documentation.

Tumor measurement and calculation of tumor growth inhibition (TGI) were performed as follows: the long and short diameters of each tumor were measured, and tumor volume was calculated using the formula: $\text{Volume} = 0.5 \times \text{long diameter} \times (\text{short diameter})^2$. The treatment/control (T/C) value was calculated based on tumor volume, using the formula: $\frac{T}{C}(\%) = \frac{\text{mean RTV of the treatment group}}{\text{mean RTV of the control group}} \times 100\%$. Relative Tumor Volume (RTV) for both treatment (T) and control (C) groups

was determined as the ratio of tumor volume after treatment to tumor volume before treatment. The Tumor Growth Inhibition Rate (TGI_{TV}) was calculated as: $TGI_{TV}(\%) = \left(1 - \frac{T}{C}\right) \times 100\%$.

Tissue distribution in tumor-bearing mice

To assess the selective accumulation and targeting efficiency of 7MW4911, CRC LS513 tumor-bearing mice were administered a single intravenous dose of 7MW4911 at 6 mg/kg when tumor volumes reached approximately 120–150 mm^3. Tumor tissues and 12 organ types, including the heart, liver, lungs, spleen, kidneys, esophagus, stomach, small and large intestines, bladder, ovary and muscle, were collected at predefined time points post-injection (0.5, 10, 24, 48, 72, 120, 168, 240, and 336 h) to evaluate drug distribution. Tissues were homogenized, and supernatants were processed for quantification of total antibody and intact ADC concentrations using a validated ELISA-based assay. Serum samples were also collected at corresponding time points to assess systemic exposure. The analytical method employed was consistent with the validated approach used in toxicokinetic bioanalysis, ensuring accuracy, precision, and reproducibility of the measurements.

Non-human primate studies

All cynomolgus monkey experiments were conducted at the Shanghai Institute of Materia Medica in accordance with standard operating procedures, approved protocols, and relevant ethical regulations, including compliance with institutional (IACUC) and international (AAALAC) animal care guidelines. Cynomolgus monkeys were administered 7MW4911 intravenously at doses of 15 mg/kg or 20 mg/kg every two weeks over an 8-week period (Days 1, 15, 29, 43, and 57, totaling five doses). Each dose group consisted of one female and one male monkey. Animals were monitored daily for clinical observations, including ophthalmology, food consumption, body weight, and body temperature. Clinical pathology assessments were conducted throughout the study and included hematology, plasma chemistry, lymphocyte immunophenotyping, immunoglobulin levels, and complement activity. Blood samples were collected at specified intervals to monitor PK and clinical parameters. A necropsy was performed one week after the final dose to assess gross pathology.

METHOD DETAILS

Antibodies

Commercial anti-CDH17 antibodies were utilized as positive controls for binding studies across different species. The LI-cadherin antibody (H-1) was procured from Santa Cruz Biotechnology (sc-393533) and was employed for mouse and rat CDH17 protein binding. The Cadherin-17 antibody from Novus Biologicals (NBP2-79857) was used for canis CDH17 protein binding. For protein expression analysis by flow cytometry, the anti-P-gp antibody (GTX42220) was obtained from GeneTex and anti-MRP2 (sc-59611) antibody was obtained from Santa Cruz Biotechnology. For IHC staining, the anti-P-gp (ab170904) and anti-ABCG2 (ab229193) antibodies were purchased from Abcam, the anti-MRP1 (sc-18835) antibody was obtained from Santa Cruz Biotechnology. The LI cadherin antibody ERP3996 was purchased from Abcam (ab109190). Monoclonal antibody 07-0663-h7, antibody for 07-0663-h7 MMAE ADC, was synthesized in-house based on the VH/VL sequence from patent WO2023107558A1 (University of California, Los Angeles). This antibody was generated in a 293 expressing system and purified using MabSelect Sure Resin (GE Healthcare Life Sciences) with a gravity column. Antibody PTA001-A4 was produced similarly, referencing the VH/VL sequence from patent US20160039933A1 for IHC-P applications. An irrelevant IgG control was produced in-house.

ELISA

For the protein binding assay, high-binding 96-well plates were coated overnight at 4°C with various human CDH17 domain His-tagged proteins, as well as mouse, rat, and canis CDH17 His-tagged proteins, sourced commercially or generated in-house. Following this, the plates were washed and blocked. Serially diluted antibodies were added to the wells and incubated for 1 h at 37°C. After washing, HRP-conjugated secondary antibodies were added and incubated for an additional hour at 37°C. Following another wash, TMB solution was added, and the optical density at 450 nm was measured using a microplate reader.

Flow cytometry

For cell-based binding analysis, flow cytometry (FACS analysis) was conducted to assess the cell binding activity of antibodies. Adherent cells were collected using Gibco Versene solution (#15040066) and adjusted to a density of 2×10^6 cells/mL in 1×PBS with 1% BSA (FACS buffer). The cells were then seeded into 96-well plates at 50 μL per well and labeled with serially diluted antibodies in FACS buffer at 4°C. After rinsing with FACS buffer, the cells were incubated with APC-conjugated goat anti-human Fc-γ fragment-specific secondary antibodies (Jackson ImmunoResearch, 109-135-098), rinsed again, and analyzed on the iQue Screener PLUS (Sartorius). All flow cytometry data were subsequently processed using GraphPad Prism.

IHC analysis

Multiple human GI cancer tissue microarrays (TMAs) were analyzed using IHC staining performed on the Leica Bond III platform. The samples underwent antigen retrieval with solution ER2 (Leica, AR9640-CN) for 20 min at 100°C, followed by blocking with

3% hydrogen peroxide for 10 min. The tissues were then incubated with a 1:100 dilution of the anti-CDH17 antibody (PTA001-A4, isotype hIgG1) for 60 min at room temperature. Detection was carried out using the Bond Polymer Refine Detection Kit (Leica, DS9800), which included anti-Human IgG (H + L)-HRP, DAB chromogenic reagents, and hematoxylin for counterstaining. The stained microarrays were scanned using a Pannoramic Digital Slide Scanner (3DHISTECH, Ltd. Pannoramic MIDI), generating high-resolution images for all samples. These images were subsequently analyzed with the HALO system (Indica Labs). A similar staining and analysis protocol was applied to xenografted tissues that were formalin-fixed and paraffin-embedded (FFPE). To evaluate target expression intensity, a histochemical scoring system (H-score) was utilized. Expression levels were classified as follows: 0 (H-score 0–14), 1+ (H-score 15–99), 2+ (H-score 100–199), and 3+ (H-score 200–300).

Bio layer interferometry

Bio-layer interferometry technology was employed to measure the binding kinetics and activity of antibodies against antigen proteins. Binding kinetics were assessed using the Octet RED96 instrument (ForteBio, Pall Corporation). 7MW4911 or Mab0727 were captured on Anti-hIgG Fc Capture (AHC) biosensor tips at a concentration of 10 μg/mL. Subsequently, the loaded samples were incubated with serially diluted soluble human or cynomolgus CDH17 proteins (Kactusbio #CDH-HM117, #CDH-CM127) at concentrations ranging from 50 nM to 3.125 nM or 200 nM–25 nM to determine the binding kinetics. The collected data were globally fitted to various binding models, specifically corresponding to a 1:1 Langmuir binding isotherm, to analyze the interaction dynamics effectively.

Development of Mab0727

Female BALB/C and SJL mice, aged 6–8 weeks, were utilized for the immunization program. Antigen CDH17 proteins were administered via intraperitoneal injection over 5–6 sessions. Mice exhibiting high serum binding capabilities received a final boost 3 days prior to euthanasia. Splenocytes were isolated and fused with the myeloma cell line P3X63-Ag8.653 using electrofusion, and HAT medium was employed for hybridoma selection. After a culture period of 10–14 days, single hybridoma clones were isolated, with antibody-producing clones identified through ELISA or FACS screening of the hybridoma supernatants. Positive clones were sequenced and subsequently expressed in the Expi293 system. Antibody candidates were evaluated for cell binding activity, internalization efficiency, and *in vitro* cytotoxicity, leading to the selection of the Mab0727 parental antibody, which demonstrated strong binding activity, high internalization potency, and effective cytotoxicity across multiple cell lines. Mab0727 parental antibody was humanized, with the removal of post-translational modification sites, specifically through the Fc L234A/L235A mutation.

Hydrophobicity evaluation by HIC-HPLC

HIC-HPLC experiments were performed using a Waters HPLC system equipped with a TSK gel Butyl-NPR column (2.5 μm, 4.6 mm × 35 mm, TOSOH). The mobile phase consisted of two components: Phase A, 20 mM histidine with 1.6 M ammonium sulfate ($(NH_4)_2SO_4$) at pH 6.0, and Phase B, 20 mM histidine at pH 6.0. Samples were prepared by diluting to 1.0 mg/mL (70 μg) with PBS and were then loaded onto the column. Gradient elution was conducted, with the mobile phase transitioning from Phase B to Phase A at a flow rate of 0.7 mL/min. UV absorbance was monitored at 280 nm. The concentration of $(NH_4)_2SO_4$ at the absorption peak time was used to assess the hydrophobicity of the samples. Hydrophobicity was calculated using the formula: $(NH_4)_2SO_4$ concentration (M) = (23−time +1.25) × 0.101. In this experimental setup, samples exhibiting an $(NH_4)_2SO_4$ concentration exceeding 0.85 M were considered hydrophilic.

Thermal stability assessment

The thermal stability of the candidate molecules was evaluated using the ProteoStat Thermal Shift Stability Assay Kit (Cat. No. ENZ-51027-K400). Protein samples were prepared at a concentration of 0.2 mg/mL in various buffers, including pH 6.0 histidine, pH 7.4 PBS, and pH 9.0 Tris. The kit buffer was diluted and mixed with the protein samples in their respective buffers. Approximately 20–25 μL of the prepared sample was dispensed into each well of a 96-well microplate. The plate was then loaded into the Biorad CFX96 Real-Time PCR system, which employed the following thermal protocol: an initial equilibration step at 25°C for 5 min, followed by an incremental temperature increase of 0.5°C every 30 s until a final temperature of 95°C was reached. The melting temperature (Tm) was determined from the thermal shift curve, where the inflection point corresponds to the temperature at which the protein undergoes a conformational change.

ADC preparation

The following commercial reagents were utilized: TCEP from Sigma-Aldrich, BL20E (including linker and payload MMAE) and MF-L6 (including linker and payload MF-6) from *Anhui Haoyuan Pharmaceutical Co., Ltd.* (China), and DMAc from Sigma-Aldrich.

For the preparation of the MMAE conjugation, TCEP was first added to the antibody at a molar ratio of 10:1 (TCEP: antibody) while maintaining a concentration of 10 mg/mL. The reaction mixture was incubated at 25°C for 120 min. Subsequently, BL20E, which contains both the linker and payload, was added and incubated with the reduced antibody at a molar ratio of 4.8:1 (BL20E: antibody) at 25°C for 60 min. The conjugated antibody was then gently mixed at 35°C for 120 min to facilitate hydrolysis. Finally, the ADC was purified using hydrophobic interaction chromatography to obtain a homogeneous ADC with a DAR of 4.

For the preparation of the MF-6 conjugation, the process began similarly by adding TCEP to the antibody at the same molar ratio (10:1) while maintaining a concentration of 10 mg/mL and incubating at 25°C for 120 min. Then, MF-L6 was introduced and incubated with the reduced antibody at a molar ratio of 4.8:1 (MF-L6: antibody) at 25°C for 60 min. Afterward, the ADC was purified by hydrophobic interaction chromatography (HIC). The final step involved gentle mixing of the ADC at 35°C for 120 min for hydrolysis, followed by ultrafiltration/diafiltration to exchange the buffer to 10 mM phosphate buffer, pH 7.4.

ADC concentration and DAR measurement

UV spectrophotometry was employed to analyze the concentration of ADCs. The ADC was diluted to approximate 0.5 mg/mL, and the corresponding buffer was diluted proportionally to serve as a blank. The protein content of the ADC was calculated using a specific formula:

$$c\left(\frac{mg}{mL}\right) = \frac{A280}{\left(\varepsilon_{\text{mAb }280}+\text{DAR}\times\varepsilon_{\text{linker payload }280}\right)}\times\left(MW(mAb)+DAR\times MW(\text{linker payload})\right)\times dilution$$

ε: Extinction coefficients

Different methodologies were utilized to determine the average DAR and drug distribution for MF-L6 and BL20E conjugates. For the MF-L6 conjugates, an analytical HIC method was implemented. The experiments were conducted using a Waters HPLC system equipped with an SHIMSEN Ankylo HIC-PH column (5 μm, 4.6 × 100 mm, SHIMADZU). The mobile phase consisted of three components: phase A, 25 mM sodium phosphate containing 1.2 M ammonium sulfate and 20 mM tetrabutylammonium bromide (pH 7.4); phase B, 25 mM sodium phosphate containing 20 mM tetrabutylammonium bromide; and phase C, 100% isopropanol. ADC samples (diluted to 1.0 mg/mL, 30 μg), a reference standard, and a blank (phase B) were loaded onto the column. The samples were eluted in isocratic mode using the mobile phase at a flow rate of 0.6 mL/min and a column temperature of 30°C. Different DARs were detected by measuring UV absorbance at 280 nm, and the content of each detected peak was quantified using the area normalization method.

For the BL20E conjugates, a similar analytical HIC method was employed. HIC experiments were performed using the same Waters HPLC system, but with a Proteomix HIC Butyl-NP5 column (5 μm, 4.6 × 35 mm, Sepax). The mobile phases were: phase A, 25 mM sodium phosphate containing 1.2 M ammonium sulfate (pH 7.0); phase B, 25mM sodium phosphate (pH 7.0); and phase C, 100% isopropanol. ADC samples (diluted to 1.0 mg/mL, 30μg), a reference standard, and a blank (phase B) were similarly loaded onto the column. The samples were eluted in isocratic mode at a flow rate of 0.8 mL/min and a column temperature of 25°C. Again, different DARs were detected by UV absorbance at 280 nm, with peak content quantified by the area normalization method.

ADC aggregation measurement

Size-exclusion chromatography-high performance liquid chromatography (SEC-HPLC) was employed to separate variants based on molecular size. The SEC experiments were conducted using a Waters HPLC system equipped with a TSKgel G3000SWXL column (5 μm, 7.8 × 300 mm, Tosoh). The mobile phase was consisted of 100 mM phosphate buffer, pH 6.8, containing 5% (v/v) isopropanol and 20 mM L-arginine hydrochloride, with a flow rate set at 0.6 mL/min. ADC samples were diluted to 1.0 mg/mL (20 μg), along with a reference standard and a blank (the mobile phase), and loaded onto the column. The column temperature was maintained at 30°C during the analysis, and UV absorbance was measured at a wavelength of 280 nm. The resulting chromatographic peaks were processed using the Empower Chromatography Data System (Waters) to determine the percentages of aggregate, fragment, and monomer species.

Cell internalization assay

In vitro antibody internalization was assessed using a commercial antibody internalization kit (Sartorius, 90565). The reagent exhibits minimal fluorescence at neutral pH and becomes highly fluorescent in acidic environments, such as those found in the lysosome/endosome pathway, thereby enabling precise detection of antibody internalization and trafficking. Briefly, the iQue Antibody internalization reagent (100 μg/mL) was mixed with test articles (100 μg/mL) at a 1:1 ratio and incubated at 37°C for 15 min. After incubation, the mixture was serially diluted 2-fold, while tumor cells expressing CDH17 were collected and seeded into 96-well plates at a density of 2×10^6 cells/mL (20 μL per well). The diluted mixture (20 μL per well) was then added, and the treated plates were incubated in a CO_2 incubator at 37°C for 24 h. The adherent cells were collected the following day, and cell analysis was performed using the iQue platform, yielding data for RL-1. Finally, results were analyzed using GraphPad Prism.

Cell cytotoxicity assay

Tumor cells with varying CDH17 expression profiles were collected and adjusted to a density of 6×10^4 to 1×10^5 cells/mL based on growth rates. The cells were then seeded into a 96-well white plate at 50 μL per well. Concurrently, diluted ADCs were added, starting at a concentration of 1.2 μg/mL or 10 μg/mL and further diluted in a 3-fold series, with 50 μL added per well. The plates were co-cultured in a 37°C CO_2 incubator for 7 days. After incubation, 100 μL of the Bio-Lite Luciferase Assay System reagent (Vazyme,

DD1201-03) was added to each well, and relative luminescence units (RLU) were measured using a Spectra M5e instrument. Cytotoxicity percentages were calculated using the formula: Cytotoxicity %= (1-Sample$_{RLU}$/Non-treated cell$_{RLU}$) × 100%. Data were analyzed using GraphPad Prism.

PK of 7MW4911 in BALB/c mice

The PK study was conducted to evaluate the drug metabolism of 7MW4911. Four female BALB/c mice, aged 6 to 8 weeks, received a single intravenous injection of 7MW4911 at a dose of 10 mg/kg. Serum samples were collected at the following time points: 0, 1, 4, 8, 24, 48, 96, 120, 144, and 192 h post-administration. To determine the drug concentration, an indirect ELISA was performed using human CDH17 his-tag protein as capturing reagent, the diluted serum was incubated with the antigen, and the anti-MF-6 antibody was employed to detect the inact ADC present in the serum. Following 1 h incubation, the plates were washed and incubated with Peroxidase AffiniPure Goat Anti-Rabbit IgG, Fcγ fragment-specific secondary antibody (Jackson ImmunoResearch, 111-035-144) for 1 h at 37°C. After additional washes, TMB solution was added, and the optical density at 450 nm (OD450) was measured using a microplate reader. The concentrations of 7MW4911 in serum at various time points were calculated based on a standard curve, and the half-life ($t_{1/2}$) was determined using the formula: $t_{1/2} = |0.693/k|$.

In vitro stability of 7MW4911 in monkey plasma

Samples were prepared by mixing the antibody or ADC with cynomolgus monkey plasma in a 1:1 ratio, resulting in a final concentration of 10 μg/mL. The mixtures were incubated at 37°C, and samples were collected on Days 0, 3, 7, 10, and 14, with sterile conditions maintained throughout the study. To quantify drug concentration, an indirect ELISA was performed using human CDH17 his-tag protein or anti-MF-6 antibody as the coating antigens for total antibody and ADC detection, respectively. The relative concentration was calculated based on baseline values. For assessing binding activity, samples were analyzed using either indirect ELISA or flow cytometry, as previously described. Data analysis was performed using GraphPad Prism.

Bystander effect

To assess the bystander effect of 7MW4911, SK-CO-1 cells were used as CDH17-positive cells, while Calu-6 cells served as CDH17-negative cells in an *in vitro* co-culture system. SK-CO-1 and Calu-6 cells were enzymatically dissociated, centrifuged, and resuspended in culture medium. SK-CO-1 cells were seeded at varying densities (3×10^4, 5×10^4, 1×10^5, 1.5×10^5, and 2×10^5 cells/mL), while Calu-6 cells were seeded at 2×10^4 cells/mL in 6-well plates and incubated overnight at 37°C with 5% CO_2. Experimental groups included Calu-6 monocultures (negative control and ADC-treated groups) and SK-CO-1/Calu-6 co-culture groups at different cell ratios. Cells were treated with 7MW4911 ADC or the corresponding antibody (5 μg/mL) and co-cultured for six days. Following incubation, cells were harvested, stained with a Trop2 monoclonal antibody, and labeled with a secondary antibody for flow cytometry analysis. The proportions of Trop2-negative (SK-CO-1) and Trop2-positive (Calu-6) cells were quantified to evaluate the bystander effect of 7MW4911 ADC in a heterogeneous tumor microenvironment.

Total antibody bioanalytical assay

Recombinant human CDH17 (extra-cellular domain) protein expressed in mammalian cells (prepared by Mabwell) was used for coating at 2 μg/mL. The plate was then washed three times with washing buffer (0.1% PBST, phosphate buffer saline containing 0.1% Tween 20) and blocked with 3% BSA/PBST for 1.5 h 7MW4911 was diluted with pooled monkey serum to concentrations of 39.063 ng/mL (anchor point), 78.125 ng/mL (LLOQ, lower limit of quantification), 156.25 ng/mL, 312.5 ng/mL, 625.0 ng/mL, 1250.0 ng/mL, 2500.0 ng/mL, and 5000.0 ng/mL (ULOQ, upper limit of quantification). These standard samples (STDs) were used to construct the standard curves. The quality control (QC) sample concentrations were 200.0 ng/mL (LQC, low QC), 1000.0 ng/mL (MQC, mid QC), and 4000.0 ng/mL (HQC, high QC). All samples, including STDs, QCs, and samples for analysis, were diluted with assay buffer (1% BSA/PBST) at an MRD (minimum required dilution) of 50 before adding to the ELISA plates at 100 μL/well and incubating at room temperature for 2 h. After washing the plate three times, goat anti-human IgG-HRP antibody (Abcam, Cambridge, UK) diluted 40,000-fold with assay buffer was added and incubated at room temperature for 1 h. Finally, tetramethylbenzidine (TMB) chromogenic substrate was added, and the reaction was terminated with 1 M phosphoric acid. Absorbance was measured at 450 nm with a reference wavelength of 650 nm using a microplate reader (Molecular Devices, SpectraMax M5, San Jose, CA, USA). The STDs with known drug concentrations were used to generate standard curves using SoftMax Pro (Molecular Devices v7.0.2 GxP) software with a four-parameter fitting method.

Conjugated antibody bioanalytical assay

Anti-MF-6 Rabbit mAb (prepared by Mabwell) was coated on 96-well ELISA plates at 2 μg/mL followed by washing the plates three times with washing buffer and blocking with 3% BSA/PBST for 1.5 h 7MW4911 ADC was diluted with pooled monkey serum to concentrations of 39.063 ng/mL (anchor point), 78.125 ng/mL (LLOQ), 156.25 ng/mL, 312.5 ng/mL, 625.0 ng/mL, 1250.0 ng/mL, 2500.0 ng/mL, and 5000.0 ng/mL (ULOQ) as the STDs. The QC concentrations were 200.0 ng/mL (LQC), 1000.0 ng/mL (MQC), and 4000.0 ng/mL (HQC). All samples, including STDs, QCs, and samples for analysis, were diluted with assay buffer with MRD = 50 before being added to the ELISA plates and incubating at room temperature for 2 h. Goat anti-human IgG-HRP antibody (Abcam, Cambridge, UK) diluted 40,000-fold with assay buffer was then added and incubated at room temperature for 1 h. Finally, TMB was

added, and the reaction was terminated with 1 M phosphoric acid. Absorbance was measured at 450 nm with a reference wavelength of 650 nm using a microplate reader. The STDs with known drug concentrations were used to generate standard curves using SoftMax Pro software with a four-parameter fitting method.

Analytical assay for free MF-6 quantification

The free MF-6 in serum was quantitatively determined by LC-MS/MS. MF-6 was diluted with pooled monkey serum (which has been treated with 4% H_3PO_4, with the ratio of 5:100 (V: V, 4% H_3PO_4:serum) to 0.0100 ng/mL (LLOQ), 0.0200 ng/mL, 0.0500 ng/mL, 0.100 ng/mL, 0.400 ng/mL, 0.600 ng/mL, 0.900 ng/mL, and 1.000 ng/mL (ULOQ) as the STDs. D5-MF-6 (MF-6 with 5 hydrogen atoms substituted by deuterium atoms, purchased from MedChemExpress) was added to all samples, including unknown samples, QCs, and STDs, as the internal standard. Methyl *tert*-butyl ether was then added to extract the MF-6 and D5-MF-6 by liquid-liquid extraction. The supernatant was centrifugally separated, dried under nitrogen, re-dissolved with 0.1% formic acid in 30% acetonitrile (v/v), and injected into the HPLC instrument (Shimadzu, LC-30AD, Tokyo, Japan) with tandem MS (AB SCIEX, Triple Quad 5500, Framingham, MA, USA) for analysis. Chromatography was performed using a Kinetex XB-C18 column (Phenomenex, 2.1 mm × 50 mm, 2.6 μm, Torrance, CA, USA). Mobile phase A was an aqueous solution containing 0.1% formic acid (v/v) and 1 M ammonium formate. Mobile phase B was 90% acetonitrile containing 0.1% formic acid (v/v) and 1 mM ammonium formate. MS was conducted using an electrospray ionization source in positive ion mode. Linear least-squares regression with a weight factor of $1/x^2$ was used to fit the standard curve. Finally, the concentrations of MF-6 in the unknown samples were calculated according to the calibration curves.

QUANTIFICATION AND STATISTICAL ANALYSIS

Statistical analyses of tumor volume and weight across groups were conducted using GraphPad Prism 9.0.0 software. One-way ANOVA was used for determining statistical significance for the relevant comparisons. For Figures 1D–1F, statistical significance was assessed using the Kruskal-Wallis test. For Figures 4C–4L, statistical significance was evaluated using an unpaired two-tailed *t*-test. For Figure S8W, the Mann-Whitney test was used. Data presented in bar charts are expressed as mean ± SEM. Statistical significance was defined as $*p < 0.05$, $**p < 0.01$, $***p < 0.001$, *and* $****p < 0.0001$, with $*p < 0.05$ considered statistically significant.